

### 3

## Long-term solar variability: What does theory say?

{ch:long\_dyn}

It bears repeating: there currently exist no consensus model for the dynamo process(es) powering the solar magnetic cycle, nor for the magnetic backreaction mechanism(s) regulating its amplitude. This evidently does not augur well for the understanding (and/or prediction) of variations of solar activity on long timescales, which is the focus of this chapter, but we shall proceed nonetheless. “Long timescale” refers here to variations of the cycle amplitude and/or duration unfolding over multi-decadal timescale or more, observational evidence for which having been presented in the preceding chapter. Of particular interest in this context are the Grand Minima episodes of strongly suppressed activity, such as the 1645-1715 Maunder Minimum (§7.2).

Grand Minima

Ref to §7.2

From the point of view of dynamo modeling, two broad classes of explanations exist for Grand Minima:

- Extreme modulation of the cycle amplitude, with the same dynamo-driven cycle perduring through a Grand Minimum, but at amplitude values too low for sunspot formation.
- Intermittency, meaning a transition between two distinct dynamo states, one being the primary “normal” cycle, and the other not necessarily cyclic but characterized by a magnetic field too weak for sunspot formation.

Thresholded Modulation

Intermittency

Extant data, as reviewed in chapter ??, currently does not allow to discriminate unambiguously between these two classes of explanations. The cyclic signal observed in the  $^{10}\text{Be}$  record across the Maunder Minimum (Beer et al., 1998, see also §X.Y herein) suggests sustained cyclic activity, as one would expect under a Grand Minimum scenario invoking amplitude modulation. On the other hand, the observed non-periodic recurrence of Grand Minima, as well as their significant variability in duration, is typically easier to produce in noise-triggered intermittency-based scenarios. Part of the

Ref to MM Fig?

difficulty goes back to the ill-understood quantitative link between sunspots and the overall strength of the dynamo-generated internal magnetic field. While the two are clearly correlated (REF previous chapter), the relationship is not linear, and is likely characterized by a threshold at low magnetic field strength.

In this context another dynamo property will play an essential role: whether or not the dynamo is self-excited, i.e., can magnetic field amplification take place from an arbitrarily weak seed field. A dynamo relying on differential rotation shear and the classical turbulent  $\alpha$ -effect is in principle self-excited, while a solar cycle model invoking, e.g., the Babcock-Leighton mechanism or flux tube instabilities for poloidal field regeneration is not. In these latter case, if the primary dynamo “turns off” for whatever reason, a distinct inductive mechanism must be invoked to restart it again.

Ref to §7.3  
Grand Maxima

The issue of the so-called Grand Maxima (see §??) is trickier. Working with historical data, lack of sunspots can be used as an unambiguous marker of Grand Minima, but no equivalent “binary” criterion exist for period of sustained, above-average activity levels. Under an intermittency-based dynamo scenario, Grand Maxima could correspond to a third, distinct dynamo state, while under the amplitude modulation view they can only be defined in terms of some (arbitrary) threshold in some magnetism-related measure.

In the remainder of this chapter a survey is presented of the various dynamo-based scenarios put forth as explanatory frameworks for long timescale variations in solar activity, including the occurrence of Grand Minima and Maxima. The various dynamo models reviewed in chapter 2 will serve as starting points towards this program. Nonlinear modulation and the complex interplay of stochastic forcing and nonlinearities leading to intermittency are first explored in §§3.1 and 3.2 using very simple low-order models, after which representative examples occurring in spatially-extended mean-field and mean-field-like dynamo models, as well as global MHD simulations, are reviewed in §3.3. Based on this survey of extant modelling framework, the issue of long-term predictability is revisited in §3.4.

{sec:amplmodul}

### 3.1 Nonlinear amplitude modulation

The dynamical backreaction of the large-scale magnetic field is an obvious mechanism to consider in exploring long timescale modulation of the primary magnetic cycle. This has been investigated in detail in the context of low-order dynamical systems, more or less inspired by truncation of the governing dynamo equations (see Tobias et al., 1995; Knobloch and Landsberg, 1996; Knobloch et al., 1998; Weiss and Tobias, 2016). Two broad classes

of amplitude modulation have been identified, based on the energetics of the long-timescale modulation: type I modulation refers to the exchange of energy between two (or more) magnetic energy reservoirs, each associated with a different equatorial parity; type II modulation refers to a modulation envelope driven by energy exchange between the magnetic field and kinetic energy of the inductive flows.

Figure 3.1 depicts schematically the workings of these two variants on nonlinear amplitude modulation. Imagine the dynamo to operate in the supercritical regime with amplitude indicated by the dot labeled A on Fig. ??A. Suppose now that the growing magnetic field leads to a reduction of differential rotation, either by direct impact of the azimuthal component of the associated Lorentz force (2.3.6), or through reduction of the Reynolds stresses powering differential rotation ( $\Lambda$ -quenching, viz. §2.3.5). The net effect can be viewed as an inexorable decrease of the effective dynamo number  $D$ . The system will gradually move from point A towards B, to a much lower magnetic amplitude, and thus much reduced Lorentz force. This

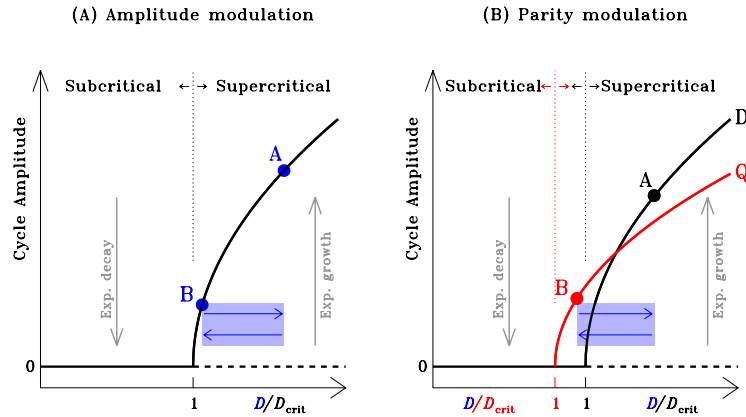


Figure 3.1 Schematic depiction of (A) amplitude modulation (Type II), and (B) parity modulation (Type I) in non-kinematic dynamo models operating not too far from criticality.

{fig:HopfAMPLmod}

will allow differential rotation to recover, leading to an increase in  $D$  and thus moving the system back to A. The dynamo number  $D$  is thus moving periodically back and forth within the range indicated by the blue box on Fig. 3.1A. If the timescale for quenching and recovery of differential rotation is longer than the (inverse) linear growth rate of the dynamo, the cycle amplitude will undergo a periodic waxing and waning, moving slowly back

and forth along the black curve from point A to B and back. This is Type II modulation.

Figure 3.1B, depicts, again very schematically, the workings of parity modulation. This materializes most readily when the lowest order equatorially symmetric (quadrupole-like) and antisymmetric (dipole-like) dynamo modes have comparable critical dynamo numbers and growth rates, as is often the case with many mean-field and mean-field-like models. This is plotted as two distinct bifurcation curves on Fig. 3.1B, labeled “D” and “Q”. Consider again a slow decrease of the dynamo number driven by a gradual reduction of differential rotation, pushing now the dominant mode (here D) from A to B, i.e., below its critical dynamo number (left-pointing blue arrow). Once differential rotation begins to recover and the effective dynamo number starts to increase (right-pointing arrow), the system resides temporarily in a regime in which the quadrupole-like symmetric mode has the largest growth rate, before returning to its dipole-like initial state. Once again a periodic modulation of the primary cycle is generated, but this time it is accompanied by a change in equatorial parity. For symmetric and antisymmetric modes having closely similar growth rates and critical dynamo numbers, this type of parity modulation can be mediated by relatively small variation of differential rotation (and also by stochastic forcing; see, e.g., Mininni and Gómez 2004; Olemskoy and Kitchatinov 2013; Hazra and Nandy 2019).

Amplitude modulation of both types can co-exist and operate simultaneously in a given dynamo system, as some of the case studies presented in §3.3 below will amply demonstrate.

Supermodulation

Type 1,2: Knobloch example, Tobias 1997

Define parity index here!

{sec:stochforc}

### 3.2 Stochastic forcing and nonlinearities

Amplitude modulation driven by stochastic fluctuations of the dynamo number, as illustrated on Fig 2.11, can lead to modulation patterns unfolding on timescales much longer than the coherence time of the fluctuations. Specific examples of this effect in mean-field dynamo models have already been presented on Figure 2.13.

A more extreme form of amplitude variation can occur if stochastic fluctuations push the solution far across the bifurcation point and into the subcritical regime; the cycle amplitude then undergoes exponential decay to the fixed-point trivial solution  $\mathbf{B} = 0$ , and the dynamo can only restart once a favorable fluctuation pushes the system back into the supercritical regime.

## (A) On–Off intermittency

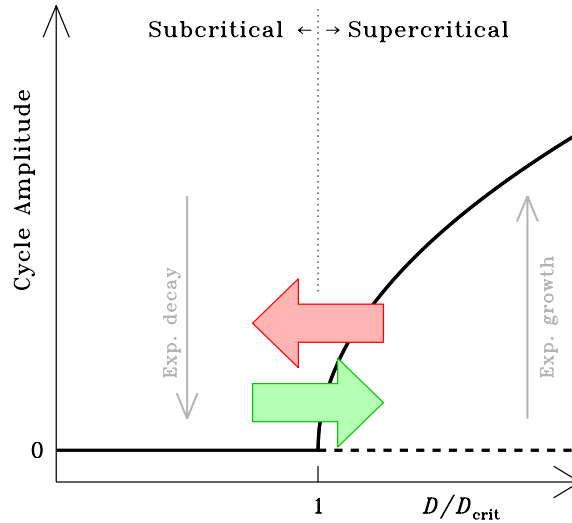


Figure 3.2 On-off of intermittency in a self-excited nonlinear dynamo models without a lower operating threshold on the field strength/cycle amplitude. Stochastic decrease of the dynamo number push the solution into the subcritical regime (red arrow) and later back into the supercritical regime (green arrow) by stochastic increase of the dynamo number.

{fig:Hopf2A}

This type of behavior, illustrated schematically on Figure 3.2, is known as *on-off intermittency* (Platt et al., 1993). It characterizes self-excited dynamo processes in which amplification remains possible even if the magnetic field falls to very low amplitude, which is the case e.g. for dynamo action driven by the turbulent mean electromotive force (§1.3.4). Under this scenario the mean duration of quiescent episodes is determined by the decay and growth timescales of the dynamo in the range of dynamo numbers spanned by the fluctuations. This represents an attractively simple explanation for Grand Minima, but is predicated on the dynamo operating relatively close to criticality.

On-Off Inter-  
mittency

The low-order model of Cameron and Schüssler (2017b) introduced in §2.4.1 offers a particularly simple example of on-off intermittency. Figure 3.3 shows a time series produced using this model. The model parameters (see eq. (2.32)) have been adjusted to fit the solar cycle, namely:  $\omega_0 = \pi/11 \text{ yr}^{-1}$

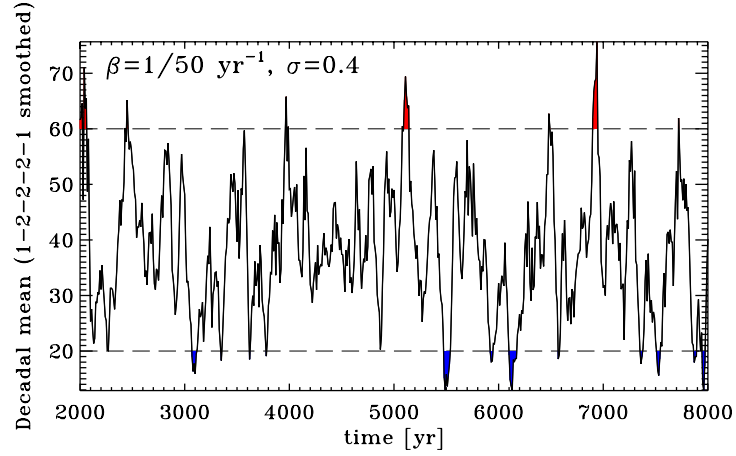


Figure 3.3 Segment of a time series of smoothed decadal mean amplitude (1-2-2-2-1 smoothing window) produced by the Cameron and Schüssler (2017b) stochastically forced low-order model, with parameter values  $\beta = 0.02 \text{ yr}^{-1}$  for the linear growth rate,  $\sigma = 0.4$  for the stochastic forcing amplitude. The horizontal dashed lines drawn at 20 and 60 indicates the lower and upper thresholds used to identify Grand Minima (colored in blue) and Grand Maxima (red) epochs. Figure produced from numerical data kindly provided by R. Cameron.

{fig:cs17intermit

for an 11-yr half-cycle,  $\gamma_i = 0$  for a amplitude-independent cycle period, and  $\gamma_r = 4.9 \times 10^{-6} \text{ yr}^{-1}$  so that the dynamical variable  $X$  has sunspot-number-like numerical values. The fluctuating behavior is then set by the linear growth rate  $\beta$ , and noise amplitude  $\sigma$ . This plot, (and many subsequent similar Figures) has been constructed such as to mimic the radioisotope-based reconstruction of solar activity levels, as discussed in §6.3 (and esp. Fig. ??).

REF to §6.3.2  
and Fig 6.7

A time series of decadal mean values  $p_n$  is first constructed from the higher temporal cadence model output, and the resulting time series smoothed using a 1-2-2-2-1 averaging filter:

$$\{\text{eq:12221}\} \quad \bar{p}_n = \frac{1}{8}(p_{n-2} + 2p_{n-1} + 2p_n + 2p_{n+1} + p_{n+2}) . \quad (3.1)$$

REF to previous  
chapter

The resulting time series of  $\bar{p}$  is plotted as the solid line on Fig. 3.3. It is characterized by substantial fluctuations including occasional excursions at very high and very low amplitude values. Following the procedure introduced in §X.Y, threshold values of  $X = 20$  and  $X = 60$  (horizontal dashed lines) are used to delineate epochs of Grand Minima and Maxima in reconstructed activity, as colored in blue and red. For proper choices of model parameters, the frequency distribution of Grand Minima duration and inter-event

waiting times constructed from the model output are both approximately exponential, as expected if the trigger is a stationary memoryless random process, and generally consistent with the corresponding distributions characterizing reconstructions based on radioisotopes, as discussed in §X.Y (see Cameron and Schüssler, 2017b, for further discussion). In this model the average duration of Grand Minima is controlled primarily by the parameter  $\beta$ , setting the linear growth rate of the dynamo. Moreover, in this model, when the dynamo is pushed in the subcritical regime, the solution is still oscillatory even though the amplitude is decreasing exponentially; residual cyclic activity during Grand Minima phases, as suggested by some radioisotope reconstructions, can thus be naturally accounted for. As explicitly demonstrated by Cameron and Schüssler (2017b), these dynamical properties carry over to a mean-field-like 1D Babcock-Leighton model, supporting the claim that these results are robust. The source of fluctuations, as captured by the parameter  $\sigma$ , is ascribed to the strong scatter in the E-W tilt of bipolar active regions (see §2.4.4, and §3.3.2 further below).

Another REF  
to §in previous  
chapter ?

The low-order model of Passos et al. (2012) introduced in §2.3.7 also exhibits on-off intermittency when subjected to stochastic forcing. The dynamical behavior is now more complex (as per Fig. 2.9) but the intermittency mechanism is still basically that illustrated on Fig. 3.2. Passos et al. (2012) impose uniformly distributed zero-mean forced fluctuations in the numerical parameter  $a$  controlling the magnitude of the magnetic backreaction on the meridional flow variable  $v_p$ . This introduces variability in the time rate of change of the flow, which directly carries over to the magnetic flux transport terms (first terms on the RHS of eqs. (2.25)–(2.26)). For an unfavorable sequence of fluctuations, the dynamo can be short-circuited and pushed into the subcritical regime. One such event is illustrated on Figure 3.4. The top panel shows time series segments of the three dynamical variables  $A$ ,  $B$  and  $v$  (see eqs. (2.25)–(2.27)) including a Grand Minimum, and the bottom panel the corresponding phase space trajectory across that Grand Minimum. On the latter, the black dashed line shows the limit cycle in the absence of stochastic forcing, the gray dots the blurring of this limit cycle when noise is introduced. The colored trajectory shows the impact of a large fluctuations triggering a high amplitude outward excursion in parameter space (blue), with subsequent collapse to the  $A = B = 0$  axis (cyan to green). Following recovery of the meridional flow variable, the dynamo grows again as at outward spiralling trajectory (yellow to red).

Under this scenario entry into a Grand Minimum is swift, while recovery to normal cycle behavior is more gradual. The strong increase in magnetic and velocity amplitudes is here a good precursor to the onset of Grand Min-

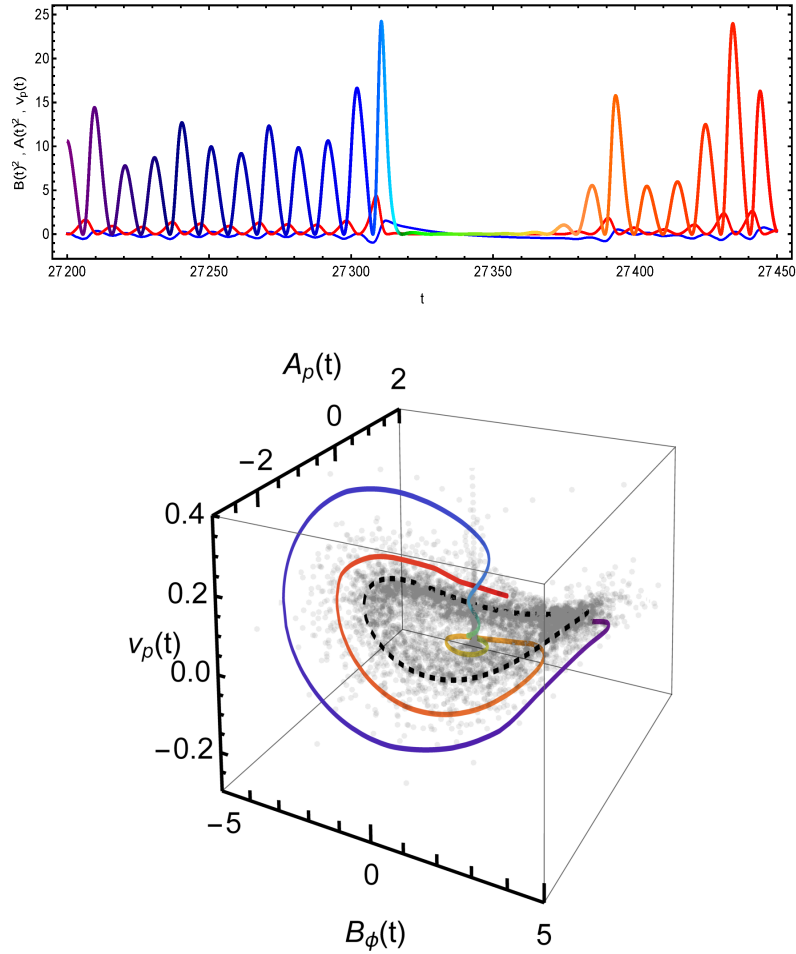


Figure 3.4 A Grand Minimum in the non-kinematic low-order dynamical model of Passos et al. (2012). The upper panel displays time series of the three dynamical variables  $A$  (poloidal field amplitude, red),  $B$  (toroidal field amplitude, purple to red), and  $v$  (meridional flow amplitude, blue) across a Grand Minimum. The bottom panel shows the same Grand Minimum, this time in the form of a phase space trajectory (see text). Adapted from Figs 8 and 11 in Passos et al. (2012).

{fig:BLMaunder}

ima, which recur aperiodically in this model. The frequency distributions of Grand Minima durations and inter-event waiting times are both approximately exponential, again consistent with a memoryless stochastic trigger.

## (B) In-Out intermittency

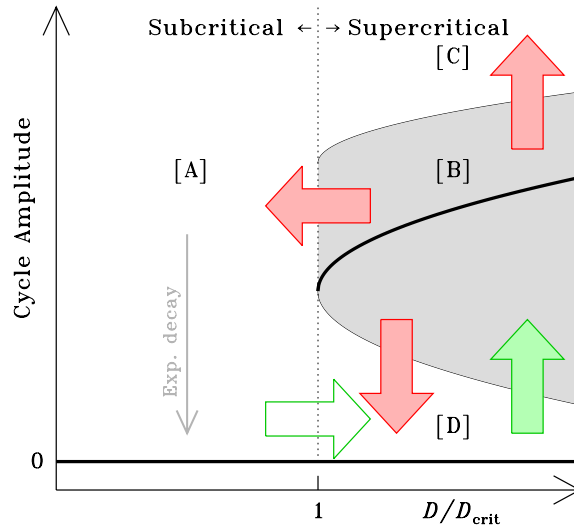


Figure 3.5 In-out intermittency in nonlinear dynamo models subjected to both upper and lower operating threshold on the field strength/cycle amplitude. The limit cycle solution (thick solid line) has a finite-sized basin of attraction, shaded in gray and labeled [B]. Here the trivial  $\mathbf{B} = 0$  fixed-point solution remains accessible in the supercritical regime, with a basin of attraction corresponding to regions [C] and [D]. Intermittent behavior can now be triggered by stochastic fluctuations either of the dynamo number (horizontal arrow), or of the cycle amplitude itself (vertical arrows).

{fig:Hopf2B}

A distinct form of intermittency can materialize in dynamos that are not self-excited, due to magnetic field regeneration being subjected to a lower operating threshold. Figure 3.5 illustrates schematically this more complicated dynamical situation. As on Fig. 3.2, the transition from the fixed-point  $\mathbf{B} = 0$  solution to a cyclic (limit cycle) state occurs when the dynamo number  $D$  exceeds its critical value  $D_{\text{crit}}$ . Here, however, at the bifurcation point the limit cycle appears with a finite amplitude, and is characterized by a finite basin of attraction (gray shading). Any initial condition within the gray-shaded area converges to the limit cycle solution (curved thick solid line), while initial solutions starting above or below converge to the  $\mathbf{B} = 0$  fixed point. This dynamical behavior characterizes dynamo models in which source terms are subjected to a lower operating threshold

on the magnetic field; Babcock-Leighton-type models (1.3.7) belong to this variety, since sunspot emergences requires a minimal strength for the participating magnetic flux ropes. In the absence of active region emergences, the regeneration of the poloidal magnetic component cannot take place, and sustained dynamo action is impossible. For specific examples of such a Babcock-Leighton models with lower operating thresholds, see, e.g., Chatterjee et al. (2004); Charbonneau et al. (2005), as well as Fig. 2.10 herein. Likewise, dynamos driven by instabilities of magnetic flux tubes (§1.3.8) also require a minimal field strength for the instability to be excited. In either cases, intermittency can now occur if some internal mechanism manages to knock the cyclic solution out of its basin of attraction.

Stochastic noise could affect the operation of such a dynamo in at least two distinct ways. If the dynamo operates close to criticality, then as with the simpler case depicted on Fig. 3.2 a fluctuation in the dynamo number can push the solution into the subcritical regime (horizontal solid red arrow on Fig. 3.5), following which the cycle amplitude will decay. Unlike for the simpler bifurcation case illustrated Fig. 3.2, here a subsequent stochastic increase of the dynamo number (open green arrow) would push the solution into region [D], which is part of the attraction basin for the  $\mathbf{B} = 0$  solution. Restart is then only possible if another source of magnetic field pushes the solution back inside the attraction basin of the cyclic solution (upward-pointing solid green arrow).

In addition, fluctuations in the cycle amplitude (of whatever origin), can push the dynamo outside of the attraction basin of the cyclic solution (vertical red arrows) even if the dynamo number remains in the supercritical regime. The magnitude of the needed fluctuations depend on the details of the dynamo model and amplitude-limiting nonlinearity considered. Note however that even very low noise level can do the trick if the dynamo operates in a regime where the solution wanders close to boundary of the attraction basin, which can happen in the chaotic regimes often accessible to strongly supercritical dynamo solutions. The mean duration of quiescent episodes under this dynamical regime is now harder quantify; as for the simpler on-off intermittency mechanism depicted on Fig. 3.2, it is controlled by the decay and growth timescales of the primary dynamo in regions [A] and [B] on Fig. 3.5, but also by the timescale(s) associated with the secondary mechanism pushing the solution back into the attraction basin ([D]→[B]).

The iterative map considered in §2.3.10 offers a particularly simple example of in-out intermittency. As the solution is pushed far into the supercritical regime, a series of period-doubling bifurcations lead to chaotic modulation, and farther in this chaotic supercritical regime the aperiodically varying am-

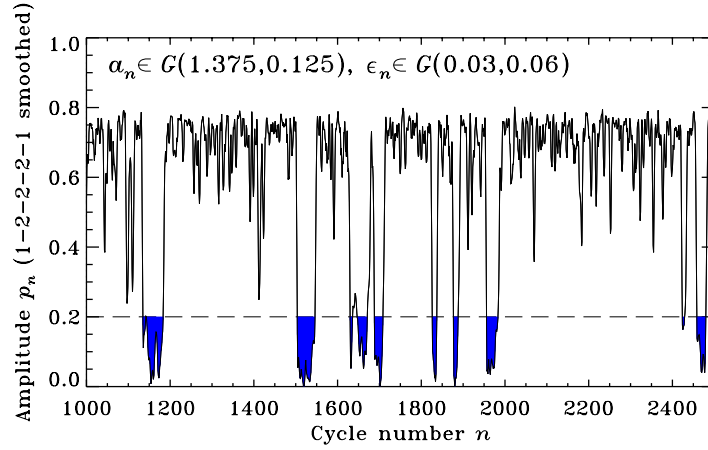


Figure 3.6 Segment of a time series of smoothed cycle amplitude (1-2-2-2-1 smoothing window) produced by the stochastically forced iterative map (3.2). The horizontal dashed line drawn at  $p_n = 0.2$  indicates the lower threshold to identify “quiescent” from “active” epochs (see text), the former being colored in blue.

{fig:stochmap}

plitude iterate wanders close to the boundary of the attraction basin (see Fig. 2.10A). Once in the chaotic regime, even low amplitude noise, meaning here noise amplitude much smaller than the amplitude iterate, can then trigger intermittency through the [B]→[C] or [B]→[D] routes on Fig. 3.5.

Figure 3.6 shows a representative time series of cycle amplitude  $p_n$ , for a stochastically-forced version of this iterative map:

$$p_{n+1} = 4a_n p_n^2(1 - p_n) + \varepsilon_n \quad n = 0, 1, 2, \dots \quad (3.2) \quad \{\text{eq:stochmap}\}$$

with

$$a_n \in G(1.375, 0.125), \quad \varepsilon_n \in G(0.03, 0.06), \quad (3.3) \quad \{\text{eq:stochmap2}\}$$

where the random deviates  $a_n$  and  $\varepsilon_n$  are extracted anew at each iterations from Gaussian distributions  $G(\mu, \sigma)$  of mean  $\mu$  and standard deviation  $\sigma$ , as indicated. Note that with these choices,  $a_n$  is very nearly always in the supercritical regime (cf. Fig. 2.10A), so the [B]→[A]→[B] channel to intermittency is essentially inactive here. In this modified form, the map parameter  $a_n$  is now subjected to stochastic fluctuations (multiplicative noise), as introduced in §2.4.2, as well as additive stochastic noise  $\varepsilon_n$ , representing the action of an additional inductive mechanism, for example a small-scale dynamo. The combined action of these two sources of stochastic forcing causes the solution to move in and out of the attraction basin of the cyclic

solution, producing quiescent phases of suppressed cycle amplitude interspersed within epochs of “normal” cyclic behavior, albeit characterized by significant cycle-to-cycle variations in amplitude. Here the system is deemed to have entered a quiescent phase when the amplitude iterate falls below  $p_n = 0.2$ , which corresponds to the lowest extent of the attraction basin for the deterministic version of this map (see Fig. 2.10). Note how the quiescent phases, colored in blue, have varying durations and show no hint of periodicity on their occurrence. Unlike on the time series of Fig. 3.3, here there are no upward excursion in cycle amplitude in the active mode of operation of the dynamo, i.e., there are no equivalents to Grand Maxima in this very simple model.

This system is characterized by an *intermittency threshold*, namely a minimal additive noise level (upper bound value on  $\varepsilon_n$  in eq. (3.3)) below which the amplitude iterate cannot climb back into the attraction basin of the limit cycle. Sufficiently far from this threshold, and provided the  $\varepsilon_n$  remain significantly smaller than the cycle amplitude  $p_n$ , the frequency distribution for the durations of quiescent phases shows little dependence on the additive noise level, except in the tail of very long duration quiescent phases. Likewise, the distribution for active phase durations is exponential and largely insensitive to the additive noise level, even though low-level noise is essential to this intermittency mechanism (see Charbonneau, 2001, 2005, for further details and illustrative examples).

{sec:cases}

### 3.3 Case studies

It is not *a priori* obvious that the production of Grand Minima and other long timescale behaviors in the various highly simplified “toy models” considered above necessarily carries over to more realistic spatially-extended solar cycle models including solar-like large-scale flows and spatially-varying inductive mechanisms. In this section we consider in some detail a few “case studies”, i.e., representative instances of such models in which counterparts to these long timescale modulation patterns and intermittent behaviors are indeed observed. Many more such examples can be found in the published literature; the selection that follows is meant primarily to illustrate the wide range of possible Grand Minima scenarios.

{ssec:alphafluct}

#### 3.3.1 Self-excited kinematic dynamos: fluctuating $\alpha$ -effect

Many extant mean-field solar cycle models achieve the production of long timescale modulation, including Grand Minima and Maxima, through forced

stochastic fluctuations of the dynamo source terms. The most straightforward avenue is on-off intermittency in mildly supercritical models, as illustrated schematically on Fig. 3.2 and captured quantitatively in the low-order dynamical system model of Cameron and Schüssler (2017b) described in the preceding section.

Our first case study is an example of this intermittency mechanism occurring in a stochastically-forced version of the mean-field dynamo model of Kitchatinov and Olemskoy (2012). This 2D kinematic axisymmetric mean field-like model solves dynamo equations equivalent to the  $\alpha\Omega$  version of eqs. (2.11)–(2.12), with a non-local surface source term capturing the regeneration of the large-scale poloidal magnetic component through the Babcock-Leighton mechanism. The model also incorporates a solar-like internal differential rotation profile and single-cell meridional flow, similar to those introduced for model BLMC in §2.2.2, but operates at low magnetic Reynolds number  $Rm = 10$ , so that the transport of magnetic flux takes place in the diffusion-dominated regime. This dynamo is self-excited, as it does not incorporate a lower magnetic field strength threshold on its poloidal source term.

The stochastically-forced version of this model, described in Olemskoy and Kitchatinov (2013), introduces fluctuations in the surface poloidal source term that depend on both space and time, a setup far more realistic physically than the simpler and more commonly adopted forced fluctuation of just the dynamo number. In keeping with the idea that their poloidal source term models the Babcock-Leighton mechanism of poloidal field regeneration through active region decay, Olemskoy and Kitchatinov (2013) set the coherence length and time of their forcing function at  $6^\circ$  and one month, typical values for the latitudinal extent and lifetime of a large active region (see their §2.3 for a full description of their forcing formalism).

Figure 3.7 shows some sample results generated with this dynamo model. The top panel shows a time-latitude diagram of the deep toroidal magnetic field, the model’s equivalent to the sunspot butterfly-diagram, and the bottom panel a 1-2-2-2-1 smoothed time series of peak integrated magnetic flux, linearly scaled to yield sunspot number-like numerical values. The model is run here in the mildly supercritical regime, so that the triggering of Grand Minima takes place through on-off intermittency (Fig. 3.2), but with an interesting new twist. The latitudinal dependence of stochastic forcing leads to the excitation of higher-order dynamo modes, which can strongly interfere with the operation of the fundamental dynamo mode even if the latter remains supercritical from the point of view of the net dynamo number (on this point see also Hoyng et al., 1994; Ossendrijver et al., 1996). This

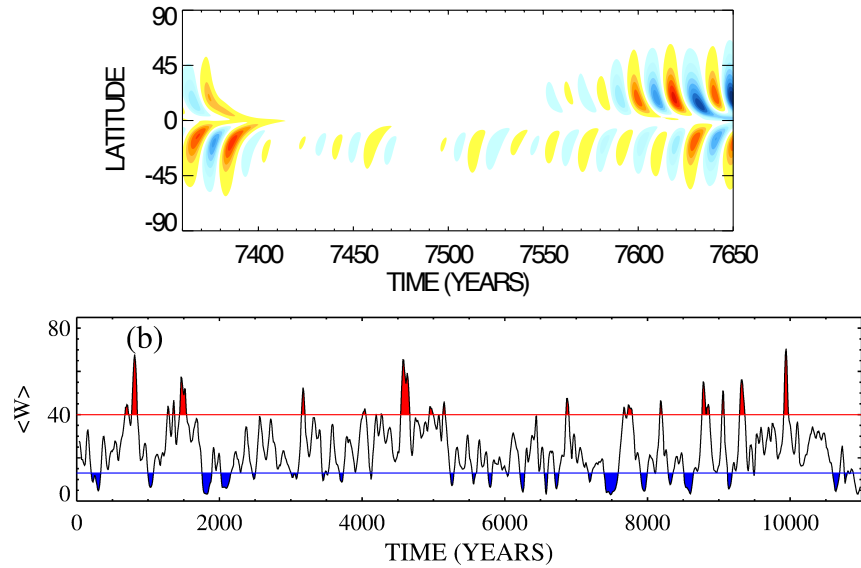


Figure 3.7 Grand Minima in the stochastically-forced Babcock-Leighton solar cycle model of Olemsky and Kitchatinov (2013). The top panel is a time-latitude diagram of the toroidal magnetic component, akin to the sunspot butterfly diagram in this model. The bottom panel shows the 1-2-2-1 smoothed time series of cycle amplitudes, in a format similar to Figs. 3.3 and 3.6. The threshold values for Grand Maxima (red) and Minima (blue) are set at values that match the fraction of time spent in these phases, as inferred from cosmogenic radioisotope-based reconstructions. Graphics kindly provided by L. Kitchatinov.

{fig:KitchOlem1}

shows up prominently on the time-latitude diagram of Fig. 3.7, as a strong hemispheric asymmetry in activity level, persisting here from the onset to the recovery phase of this model Grand Minimum. Note also the residual cyclic activity throughout the Grand Minimum, here restricted to the Southern hemisphere.

Interestingly, the frequency distribution of Grand Minima durations, as reconstructed from the bottom panel of Figure 3.7, shows a hint of bimodality akin to that characterizing some radioisotope reconstructions. As with the simple low-order model of Cameron and Schüssler (2007), the mean duration of Grand Minima is primarily set by the linear growth rate of the dynamo, and a solar-like distribution results from operating the model in the mildly supercritical regime. The inter-event waiting time distribution is again approximately exponential, as expected from a stationary memoryless random process.

REF to Fig  
in previous  
chapter?

For other examples of intermittency through stochastic forcing of a self-excited dynamo, see also Ossendrijver et al. (1996); Tworkowski et al. (1998); Moss et al. (2008); Usoskin et al. (2009).

### 3.3.2 Non-self-excited dynamos: dual source terms

{ssec:2alphafluc

In dynamo models that are not self-excited, recovery from a Grand Minimum may require a second inductive mechanism to push the primary dynamo back above its operating threshold (upward-pointing green arrow on Fig. 3.5). Our next case study offers an example of such a dual-dynamo solar cycle model.

The kinematic 2D mean-field-like model of Passos et al. (2014) invokes the Babcock-Leighton mechanism of poloidal field regeneration for its primary dynamo, and uses a solar-like differential rotation and a quadrupolar meridional flow (single cell per meridional quadrant), as described in Chatterjee et al. (2004). In the Passos et al. (2014) implementation, the Babcock-Leighton mechanism operates in a finite range of toroidal field strengths  $10^3 \leq B_\phi \leq 10^5$  G; its dynamical behavior is thus akin to Fig. 3.5, i.e., the dynamo has a finite basin of attraction in the supercritical regime. To allow restart of the primary dynamo, a secondary dynamo relying on the turbulent electromotive force associated with convection is added within the bulk of the convection, quenching at a field strength  $B_\phi > 10^4$  G (on such “dual-dynamos”, see also Dikpati and Gilman, 2001; Mason et al., 2002; Cole and Bushby, 2014). Forced stochastic fluctuations are imposed on either or both of the two dynamo numbers controlling the strength of the poloidal field regenerative terms, i.e., the stochastic driver affects only the  $T \rightarrow P$  portion of the dynamo loop. The onset and recovery from a Grand Minima thus follows the [B]→[A]→[D]→[B] path on Fig. 3.5.

Figure 3.8 depicts a typical Grand Minimum arising in this dual-dynamo model. The top panel is a time-latitude diagram of locations of bipolar magnetic region emergences, and the bottom panel shows the corresponding time-latitude diagram for the deep-seated toroidal magnetic field generating these emergences. Note how strong hemispheric asymmetries and residual cyclic activity is observed across the Grand Minima, analogous to the Maunder Minimum (cf. Fig. 4.14A).

Ref Fig 4.14A

The magnitude and partial overlap in the operating range of the two dynamo source terms is important and requires some fine tuning for the desired behavior to materialize. The basic (non-fluctuating model) introduces a turbulent  $\alpha$ -effect of a magnitude low enough to cause minimal changes in the magnetic cycles generated by the Babcock-Leighton source term in its absence. The frequency and mean duration of Grand Minima

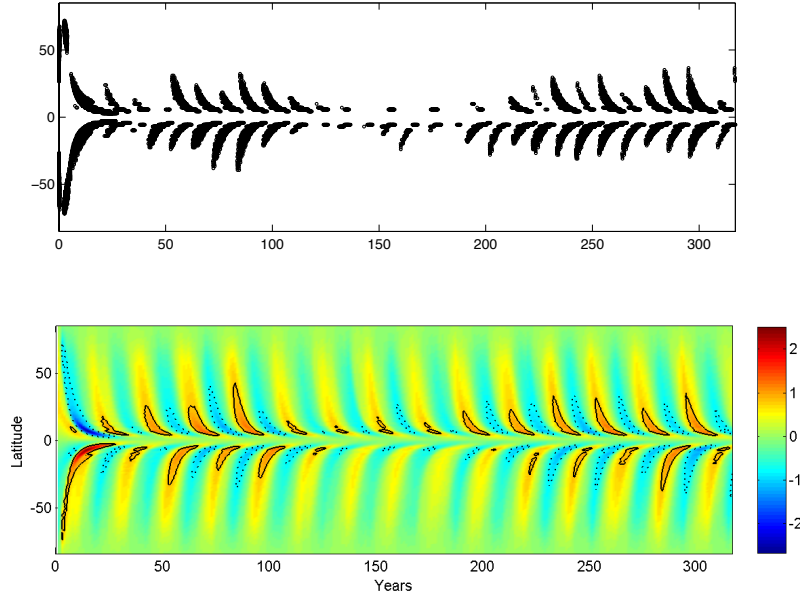


Figure 3.8 A Grand Minimum in the stochastically-forced dual-dynamo model of Passos et al. (2014), a 2D axisymmetric kinematic mean-field-like dynamo combining a Babcock-Leighton surface poloidal source term and a classical  $\alpha$ -effect distributed in the convection zone. Time-latitude diagrams of bipolar magnetic region emergences (top panel) and deep-seated toroidal magnetic field (bottom panel) are shown, spanning a Grand Minimum episode. The first 30 simulated years are still relaxing the (arbitrary) initial condition.

{fig:GMPassos14}

episodes is found to depend on the magnitude and fluctuation levels of both of these poloidal source terms. A supercritical Babcock-Leighton dynamo and strongly fluctuating mean-field  $\alpha$ -effect leads to long Grand Minima, while a mildly critical Babcock-Leighton dynamo and smaller fluctuations in the mean-field  $\alpha$ -effect yields shorter and more frequent Grand Minima. In all cases the occurrence of Grand Minima is aperiodic, as expected from a stochastic trigger.

For the solution displayed on Figure 3.8, this dual-dynamo system never entirely shuts off, as evidenced by the sustained regular polarity reversals of the deep toroidal field (bottom panel). The turbulent  $\alpha$ -effect is preventing the primary dynamo from becoming strongly subcritical, maintaining it instead close to criticality. Grand Minima in this model are perhaps better

characterized as being caused by a form of self-regulating amplitude modulation combined with a threshold effect, rather than true intermittency.

In solar cycle models relying on the Babcock-Leighton mechanism of polar field reversal and regeneration, the variability in the emergence rates and physical properties of bipolar active regions amounts to a source of strong stochasticity in the  $T \rightarrow P$  segment of the dynamo loop. Figure 2.14 already demonstrates that a single active region with extreme characteristics (such as a large magnetic flux and tilt angle departing strongly from Joy's law) can strongly alter the buildup of the surface dipole, and consequently the amplitude of the subsequent magnetic cycle. Such occurrences have been observed on the sun (Cameron et al., 2014), and are often invoked as the physical origin of the strong stochasticity introduced in an ad hoc manner in many extant Babcock-Leighton solar cycle models of varying levels of complexity. The models of Cameron and Schüssler 2017b, Olemskoy and Kitchatinov 2013 and Passos et al. 2014, just considered above, are all cases in point.

Our next case study builds on the  $2 \times 2$ D solar cycle model of Lemerle and Charbonneau (2017) described in §2.4.4. This kinematic dynamo model incorporates a detailed description of surface flux evolution and bipolar magnetic flux emergence and surface flux evolution, the physical characteristics of the latter being drawn from statistical distributions built from observed solar active regions. In some rare and extreme cases, the negative impact of a large, “rogue” bipolar active region on the global dipole can be strong enough to shift the phase relationship between the surface dipole and internal magnetic field to the point of derailing the cycle and effectively pushing the model into the subcritical regime ( $[B] \rightarrow [A]$  red arrow on Fig. 3.5; see §X.Y in Nagy et al. 2017 for a specific example).

As with the simpler mean-field-like model of Passos et al. (2014), once the dynamo shuts off and enters a Grand Minimum, a secondary dynamo process is required to kickstart it again for recovery to normal cyclic behavior. Once again a weak mean-field  $\alpha$ -effect can achieve the desired effect. Under “normal” conditions the magnetic field generated by the (primary) Babcock-Leighton dynamo quenches the  $\alpha$ -effect of the (secondary) turbulent dynamo. But once the primary dynamo shuts off, the magnetic field decays under the operating threshold of the turbulent  $\alpha$ -effect, which then turns on and pushes the magnetic field back above the operating threshold of the primary dynamo, and normal cyclic behavior resumes; as with the Passos et al. (2014) model just considered, relatively fine tuning of the magnitude and quenching levels of the two source terms is required to obtain the desired behavior.

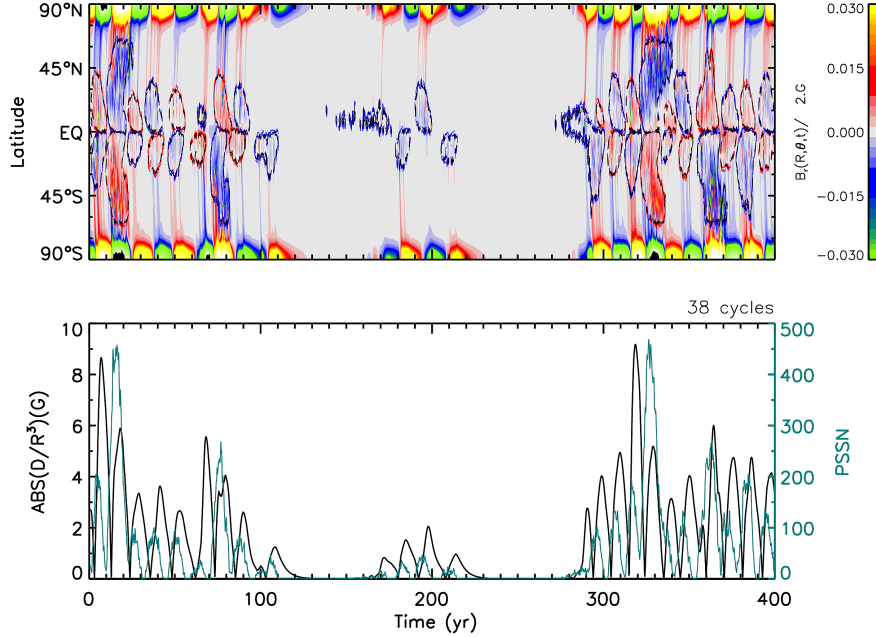


Figure 3.9 A Grand Minimum in the Lemerle and Charbonneau (2017) Babcock-Leighton dynamo model including a secondary turbulent  $\alpha$ -effect concentrated at the bottom of the convection zone. The top panel shows a time-latitude diagram of the surface radial field, on which are superimposed isocontours of the surface density of emerging bipolar magnetic regions. The bottom panel shows time series of pseudo-sunspot number and surface dipole moment. Adapted from Fig. 2 in Ölçek et al. (2019).

{fig:GMDeniz}

Figure 3.9 displays a Grand Minimum occurring in this model, in the form of a surface time-latitude diagrams of the zonally-averaged surface radial field component with superimposed isocontours for the density of emerging bipolar magnetic regions (top), and time series of pseudo-sunspot number and surface dipole moment (bottom). This Grand Minimum is characterized by a failed restart at  $t \simeq 170$  yr, during which buildup and reversal of the surface dipole resumes for four half-cycles, but there is otherwise no clear periodic signal across this extended (duration  $\sim 200$  yr) quiescent period. Note also the intermittent surges of mid-latitude activity; in this model, these sometimes persist for many successive cycles, and can be interpreted as the model's equivalent of Grand Maxima.

Strong hemispheric asymmetries are present before entering and upon exiting the extended Grand Minimum. As with the stochastically forced mean-

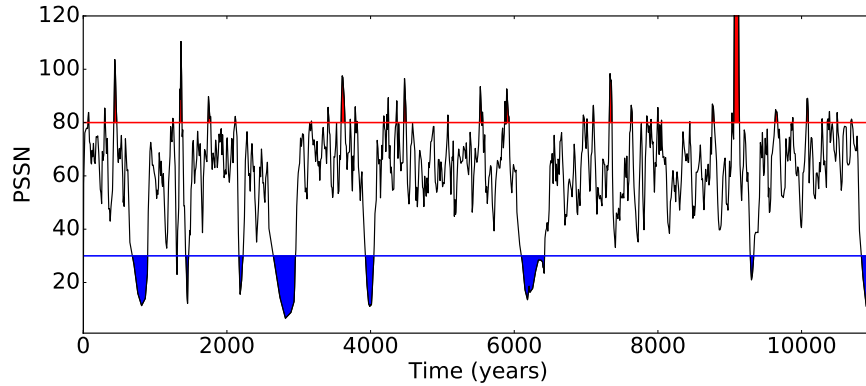


Figure 3.10 Time series of 1-2-2-2-1 smoothed cycle amplitudes in an extended simulation run of the Lemerle and Charbonneau (2017) Babcock-Leighton dynamo model including a secondary turbulent  $\alpha$ -effect. As in earlier such Figures Grand Maxima and Minima are colored in red and blue respectively. The threshold value used to identify the latter is chosen so as to reproduce cosmogenic radioisotope-based estimates for the fractional time spent in Grand Minima states. Note the extreme Grand Maximum at  $t \simeq 9100$  yr. Simulation and graphics courtesy of D. Ölçek.

{fig:GMDenizts}

field-like solutions of Fig. 3.7, stochastic forcing is here decorrelated between hemispheres, as it results from random variations in the physical characteristics of simulated emerging BMRs. However here hemispheric asymmetries are also induced by the interaction of the turbulent  $\alpha$ -effect-driven dynamo, for which the fastest growing linear mode is steady and equatorially symmetric. This explains the dominance of negative magnetic polarity throughout the Grand Minimum. See Ölçek et al. (2019) for further details on the interaction between the two dynamos operating concurrently in these simulations.

Figure 3.10 shows a time series of smoothed cycle amplitudes for the same model run as on Fig. 3.9, but over a  $10^4$  yr time span, in the now usual format. Grand Minima and Maxima recur aperiodically, and with former showing a much wider range of durations than the latter. Here once again the onset of Grand Minima and Maxima is driven by memoryless stochastic process, leading in both cases to inter-event waiting time distributions that are exponential in form. The duration of Grand Minima is set by two factors: the decay time of the residual large-scale magnetic field once the dynamo shuts off determines at which point quenching of the  $\alpha$ -effect will vanish; and the growth time of the associated  $\alpha\Omega$  dynamo process. For the solutions displayed on Fig. 3.9, the former dominates and effectively sets the mean

duration of Grand Minima phases. Their wide range of durations ultimately reflects the state of the internal field at the time the primary Babcock-Leighton dynamo shuts off.

For other examples of in-out intermittency in non-self-excited dynamos through the interplay of dual magnetic induction mechanisms, see Schmitt et al. (1996); Ossendrijver (2000b); Charbonneau et al. (2004); Karak and Choudhuri (2013); Hazra et al. (2014a).

{ssec:cmfluct}

### *3.3.3 Fluctuating meridional flow*

In dynamo models characterized by spatially segregated inductive source regions, any stochastic or deterministic (nonlinear) variation of the transport process linking the source regions can alter the dynamo loop, and in some cases shut it off altogether. Our next case study, the solar cycle model of (Choudhuri and Karak, 2012, see also Karak 2010; Karak and Choudhuri 2013) exemplifies the production Grand Minima through stochastic variations of the meridional flow amplitude in a Babcock-Leighton solar cycle model.

The dynamo model used by Choudhuri and Karak (2012) is described in detail in ?. It is a 2D axisymmetric kinematic mean-field-like model similar to model BLMC introduced in §2.2.2, but with the Babcock-Leighton mechanism modeled as a conventional subsurface  $\alpha$ -effect term on the RHS of the evolution equation for the poloidal magnetic component. Active region emergences are mimicked by depositing toroidal magnetic fields in the subsurface layers whenever the deep-seated toroidal field at the same latitude exceeds some preset threshold. The model uses a solar-like differential rotation profile and a quadrupolar meridional flow, with a single flow cell per meridional quadrant. While a lower threshold exists on emergences, there is none on the  $\alpha$ -effect itself, which can also operate on any diffuse magnetic field present in the subsurface layers, a feature important in what follows.

The simulations described below result from operating the model in the the so-called diffusion-dominated regime (see Yeates et al., 2008, and discussion therein), in which case a positive correlation materializes between the speed of the meridional flow and the amplitude of pseudo-sunspot cycles. Such a correlation makes it possible to make a model-dependent inference of past meridional flow variations from the known amplitude and duration of sunspot cycles (see, e.g. Lopes and Passos, 2009; Karak, 2010).

Fit a Gaussian, then run temporally-extended simulations.

Not intermitency; GM produced by the combined effects of a threshold

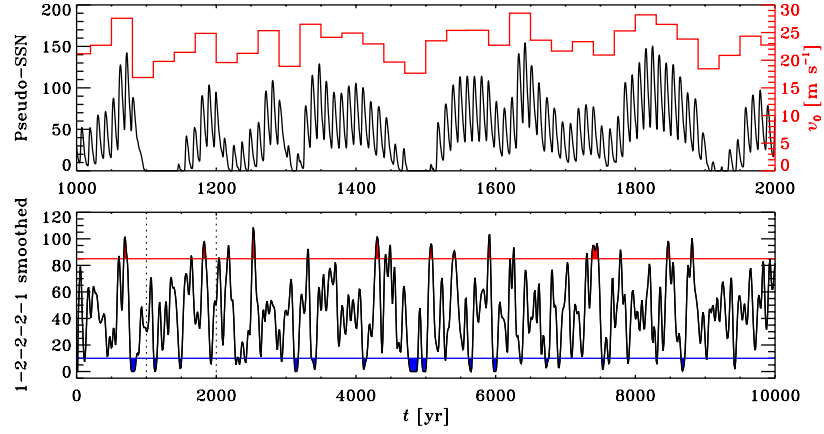


Figure 3.11 Grand Minima in the axisymmetric kinematic BL model of Karak and Choudhuri (2013), including forced stochastic variations of the meridional flow. The top panel shows time series of pseudo-sunspot number (black) and meridional flow speed parameter (red) over a 1000 yr time span. The bottom panel shows the 1-2-2-2-1 smoothed decadal mean over  $10^4$  yr, with Grand Maxima and Minima indicated in red and blue, as on previous similar plots. The dotted lines delineate the time interval corresponding to the top plot. Figure generated from numerical data kindly provided by B.B. Karak.

{fig:KC13}

on sunspot emergence and amplitude modulation by forced CM variations (Karak10 Fig 3)

Exponential distributions of GM duration and interevent wait time as expected from meoryles stochastic trigger.

Need long coherence time to obtain GM; hard to justify if flow variations are driven by convective turbulence with coherence time of a few months; But model is kinematic; such long timescale variations perhaps driven by magnetic backreaction. Investigation of this mechanism with nonkinematic

### 3.3.4 Self-excited dynamos: nonlinear magnetic backreaction on differential rotation

In all of the above case studies, cycle fluctuations are generated in the  $P \rightarrow T$  segment of the dynamo loop. We now turn to the  $T \rightarrow P$  segment, specifically the nonlinear magnetic backreaction on differential rotation. As discussed already in ??, this mechanism can achieve saturation of the dynamo at fixed cycle amplitude; however, in the low Prandtl number regime, it can also generate extreme amplitude modulation which, in conjunction with

a field strength threshold on sunspot formation, can offer a viable physical explanation for Grand Minima and Maxima.

Our first case study in this family is the dynamo model described in Bushby (2006). This is a non-kinematic but otherwise conventional self-excited 2D axisymmetric  $\alpha\Omega$  dynamo model, relying on differential rotation shear and the turbulent  $\alpha$ -effect as inductive mechanisms. The model uses a solar-like internal differential rotation profile, a negative (N-hemisphere)  $\alpha$ -effect concentrated at low latitudes, and a magnetic diffusivity dropping rapidly below the convection zone, yielding an interface-like dynamo. The nonlinear backreaction on differential rotation uses the strategy outlined in §2.3.6, namely solving only for the variations of the differential rotation with respect to an imposed solar-like profile (viz. eq. (2.23)), via the solution of a reduced dynamical essentially identical to eq. (2.24).

Figure 3.12 shows a set of magnetic energy time series generated using this model, obtained for various combinations of dynamo and Prandtl numbers, as labeled. Recall (from §2.3.6) that the latter sets the timescale over which magnetically-induced variations of large-scale flows are attenuated. At low dynamo number  $D$  and Prandtl number  $\text{Pm} \sim 1$ , the dynamo develops a constant-amplitude cycle (not shown), here with a period  $P \simeq 10^{-2}\tau$ , where  $\tau$  is the magnetic diffusion time (viz. eq. (1.9)). This primary cycle remains in the low-Pm regime, but there now also appears a modulation on a timescale much longer than the primary cycle, with period given approximately by  $P/\text{Pm}$  (panel A). This modulation becomes chaotic as the dynamo is pushed farther into the supercritical regime (panel B). At fixed dynamo number, the modulation period increases as Pm decreases (cf. panels C and D). Parity (red) modulation also occurs in all solutions, becoming quite irregular in the more supercritical solutions and/or at low Prandtl numbers. without any preferred symmetry emerging. Careful comparison of the black and blue time series on Fig. 3.12 reveals that the kinetic energy associated with the flow perturbation lags temporally the magnetic energy. While the overall amplitude of differential rotation variations increases with decreasing Prandtl number on long timescales, the amplitude of torsional oscillations on the timescale of the primary cycle vary proportionally with Pm. Referring back to the simple low-order order model of §3.1, these non-kinematic solutions typically exhibit concurrently both Type I and Type II patterns of amplitude modulation.

For the strongly modulated solution of Fig. 3.12D, it is tempting to identify the modulation phases of very low magnetic energy ( $\text{ME} \leq 0.05$  say) with Grand Minima. Entry and exit from these Grand Minima is gradual and often accompanied by strong hemispheric asymmetry, a natural consequence of

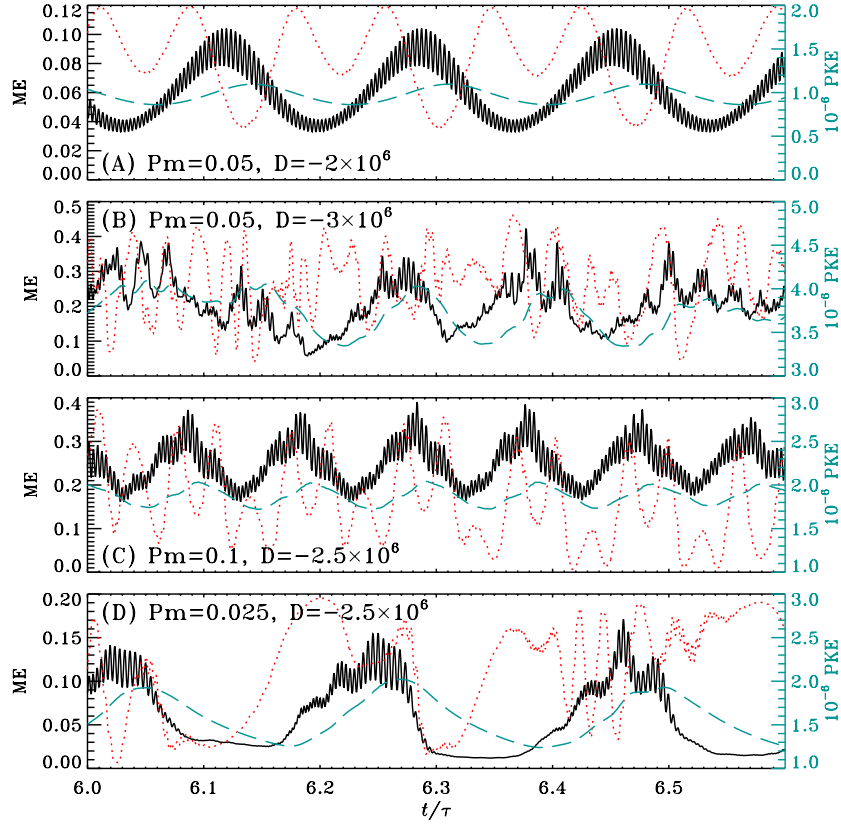


Figure 3.12 Cycle amplitude modulation in the non-kinematic  $\alpha\Omega$  mean field model of Bushby (2006). The four panels show time series of magnetic energy (ME, in black), perturbation kinetic energy (PKE, in blue-dashed) and parity (red-dotted, scaled from  $[-1, 1]$  to the vertical extent of each plot), for different combinations of dynamo and Prandtl numbers, as labeled. Time is in unit of the magnetic diffusion time, and the critical dynamo number for the range of model parameter values explored is  $\simeq -1.5 \times 10^6$  for  $Pm \sim 1$ . Plotted from numerical data kindly provided by P. Bushby.

{fig:nkin1}

parity modulation. Although not obvious on Fig. 3.12D, the primary cycle does perdure through Grand Minima, albeit at very low amplitude. In this parameter regime Grand Minima tend to recur quasi-periodically, on a timescale inversely proportional to the Prandtl number, their roughly con-

stant duration being set by the time required to dissipate the flow variations induced by the Lorentz force.

In the strongly chaotic solution of Fig. 3.12B it is also certainly possible to identify phases of very low magnetic energy with Grand Minima. They are now markedly aperiodic and not as well delineated as for the solution plotted on panel D. This solution also exhibits, on very long timescales, an additional modulation pattern whereby both magnetic and perturbation kinetic energy undergo a rapid upwards excursion by over two orders of magnitude, followed by slower recovery to the “basal” chaotic state. This could be interpreted as Grand Maxima in this dynamo model. In all these solutions, introduction of  $\alpha$ -quenching as an additional amplitude-limiting regularity tends to stabilize the modulation patterns, in both magnetic energy and parity.

Figure 3.13 shows the behavior of a similar non-kinematic 2D axisymmetric dynamo model, this time using a full  $\alpha$ -tensor extracted from the global MHD “millennium” simulation discussed in §?? (see in particular Fig. 2.5). The top panel shows time series of magnetic energy (black) and parity (red) over a timespan covering a Grand Maximum immediately followed by a Grand Minimum. The bottom panel shows the corresponding time-latitude diagram for the toroidal magnetic component at mid-depth in the convection zone. As in the Bushby (2006) model just considered, at Prandtl number  $Pm \simeq 1$  this self-excited dynamo settles into a fixed-amplitude cycle (see Fig. 2.8), but for  $Pm$  significantly below unity develops a modulation of the cycle amplitude on timescales much longer than the cycle period, with ubiquitous modulation of the solution parity. Here the solution is in a symmetric (quadrupolar-like) state across the high-amplitude phase and subsequent decrease into a very low amplitude, Grand Minimum-like regime, but then re-emerges in an antisymmetric, dipole-like configuration. Similar parity modulation across Grand Minima has been observed in other non-kinematic models of varying levels of complexity (see, e.g., Tobias, 1997; Beer et al., 1998; Sokoloff and Nesme-Ribes, 1994). In this model the modulation period is found to increase with decreasing  $Pm$ , the ratio scaling approximately as  $Pm^{-1}$ .

Figure 3.14 shows a time series of magnetic energy for the same solution, but now over a  $\sim 10^4$  yr time span, in which the primary cycle has been removed so that only the modulation amplitude remains. Threshold values have been set to identify Grand Minima (blue) and Maxima (red), with values such that the percent time spent in Grand Minima and Maxima is approximately the same as inferred from the radioisotope record. Although not particularly obvious on Fig. 3.14, the inter-event waiting time distributions for Grand Minima and Maxima are both well approximated by exponentials,

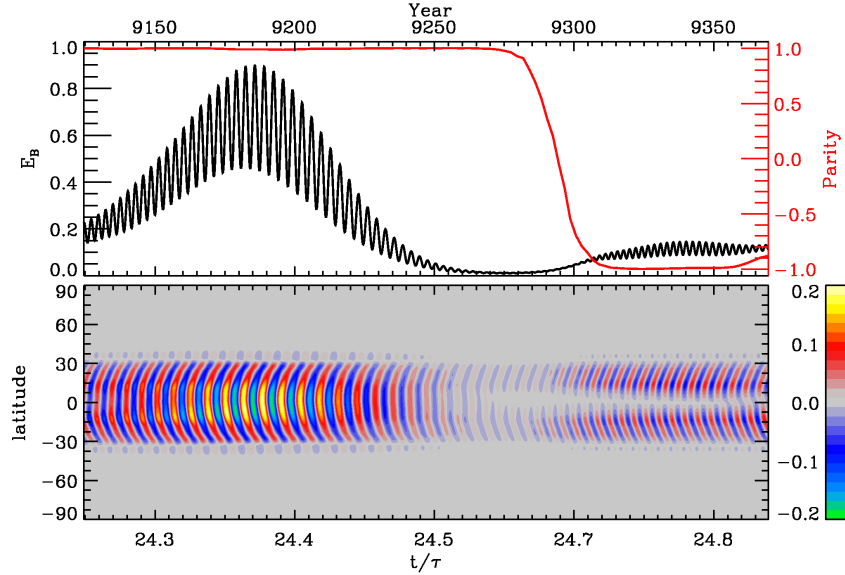


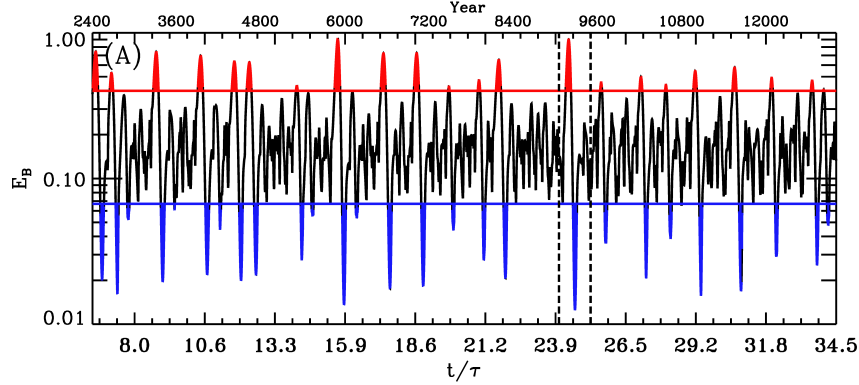
Figure 3.13 Parity modulation in a non-kinematic 2D axisymmetric  $\alpha^2\Omega$  mean-field model. This is a low Prandtl number, supercritical solution ( $\text{Pm} = 10^{-2}$ ,  $D = 5.25 \times 10^5$ ) exhibiting chaotic modulation (cf. Fig. 3.12D).

{fig:nkin2}

even though the modulation is here entirely deterministic, i.e., characterized by infinite “memory”.

As noted in 2.1.6, the dynamo-generated magnetic field impacts differential rotation not just through the large-scale Lorentz force, but also through the modulation of hydrodynamical forcing of differential rotation (see Fig. ??). In the mean-field context, the magnetically-mediated reduction of Reynolds stresses, otherwise known as  $\Lambda$ -quenching (see Kitchatinov and Rüdiger, 1993; Kitchatinov et al., 1994, also §2.3.5 herein). Küker et al. (1999) have investigated the production of strong amplitude modulation and Grand Minima via this mechanism. If  $\Lambda$ -quenching is strong and dominant over other amplitude-limiting mechanisms, quasiperiodically-recurring Grand Minima are produced in the low ( $10^{-1}$ ) Prandtl number regime. Entry into and recovery from Grand Minima is gradual, and in their model is accompanied by a reduction of the cycle period by factors ranging from 2 to 4. Lowering the Prandtl number to  $10^{-2}$  yields even more extreme variations, with Grand Minima becoming very rare events.

For other examples of extreme cycle amplitude modulation through non-



{fig:nkin3} Figure 3.14 Modulation envelope for the cycle amplitude over a  $10^4$  yr time span in the non-kinematic  $\alpha^2\Omega$  mean-field solution of Figure 3.13. Compare to Figs. 3.3, 3.6, 3.7 (bottom), and 3.10.

linear magnetic backreaction on large-scale flows in a self-excited dynamo, see also Brooke et al. (1998); Pipin (1999); Kitchatinov et al. (1999); Brooke et al. (2002); Phillips et al. (2002).

{ssec:MHDintermitt}

### 3.3.5 Global MHD simulations

Global magnetohydrodynamical simulations of turbulent thermally-driven convection and dynamo action (see §2.1) in principle incorporate many of the mechanisms and interplays of mechanisms that can lead to extreme amplitude modulation and/or intermittency. In particular, nonlinear backreaction on flows and a strongly fluctuating turbulent electromotive force are both present, and are captured in a dynamically consistent manner at all spatial and temporal resolved by the simulations.

Figure 3.15 shows a segment of a simulation run from the global MHD simulation discussed in Augustson et al. (2015). This is a high-resolution MHD simulation using the ASH code (REFs) with slope-limited diffusion, going under the code name K3S. This low Rossby number simulation operates at three times the solar rotation rate, and generates a solar-like differential rotation profile as well as a regular large-scale magnetic cycle with full magnetic period of 6.2yr and dipole-like equatorial parity. The large-scale magnetic fields accumulates at the base of the domain and develops unipolar large-scale polar caps, as well two equipartition-strength wreath-like twisted toroidal flux systems at mid-latitudes, which migrate equatorward in the

course of each half-cycle. Large magnetically-mediated modulation of differential rotation develop in the course of the magnetic cycle, with the mid-latitude large-scale shear reduced by as much as 60% at cycle peak. This deterministic modulation of differential rotation is found to play a key role in the process of magnetic polarity reversal (on this see also Strugarek et al., 2017).

The K3S simulation also produced a Grand Minimum-like event, lasting some 5 half-cycles, which appears to result from a form of parity modulation. The top panel of Figure 3.15 shows a time-latitude diagram of the zonally-averaged radial magnetic component at depth  $r/R = 0.75$ . The disruption of the cycle at low latitudes between  $t = 34$  and 50 yr is quite striking. The total magnetic energy integrated over the simulation domain (middle panel) diminishes only slightly during the event, although this reflects in part the persistence of the strong magnetic fields sustained at high latitudes in this simulation; if the volumetric integration is restricted to  $\pm 40^\circ$  latitude, the drop in magnetic energy becomes more conspicuous (orange time series). The disruption of the basic cycle is associated with the excitation of modes of even equatorial parity, with concomitant decrease of odd-parity modes. This is shown on the bottom panel of Fig. 3.15, displaying time series of magnetic energy associated with axisymmetric ( $m = 0$ ) modes of odd (red) and even (blue) equatorial parity. These time series are constructed from the radial magnetic field component at depth  $r/R = 0.75$ . Up to  $t \simeq 33$  yr the odd parity had remained dominant, but then switches rapidly to a mixture of odd and even parity which perdure throughout the event. Such a change in the repartition of magnetic energy between modes of opposite parity, while the total energy remains approximately constant, is reminiscent of the Type I nonlinear modulation described in §3.1. Recovery to dominant odd parity takes place more gradually across the Grand Minimum, but power in even parity modes remains elevated for many cycles following the end of the event. The detailed analysis carried out by Augustson et al. (2015) reveals that both the entry and exit from the Grand Minimum are coincident with the appearance of significant power in the non-axisymmetric ( $m \neq 0$ ) modes (see their Fig. 7b).

The K3S simulation of Augustson et al. (2015) just discussed arguably offers, at this writing, the closest analog of a Grand Minimum occurring in a global MHD simulation. Other similar simulations do offer examples of other potentially relevant mechanisms for disrupting magnetic cycles developing therein. Figure 3.16, taken from Lawson et al. (2015), depicts the apparent disappearance of the large-scale magnetic cycle in a EULAG-MHD simulation akin to that discussed in §2.1. The top time-latitude diagram shows the

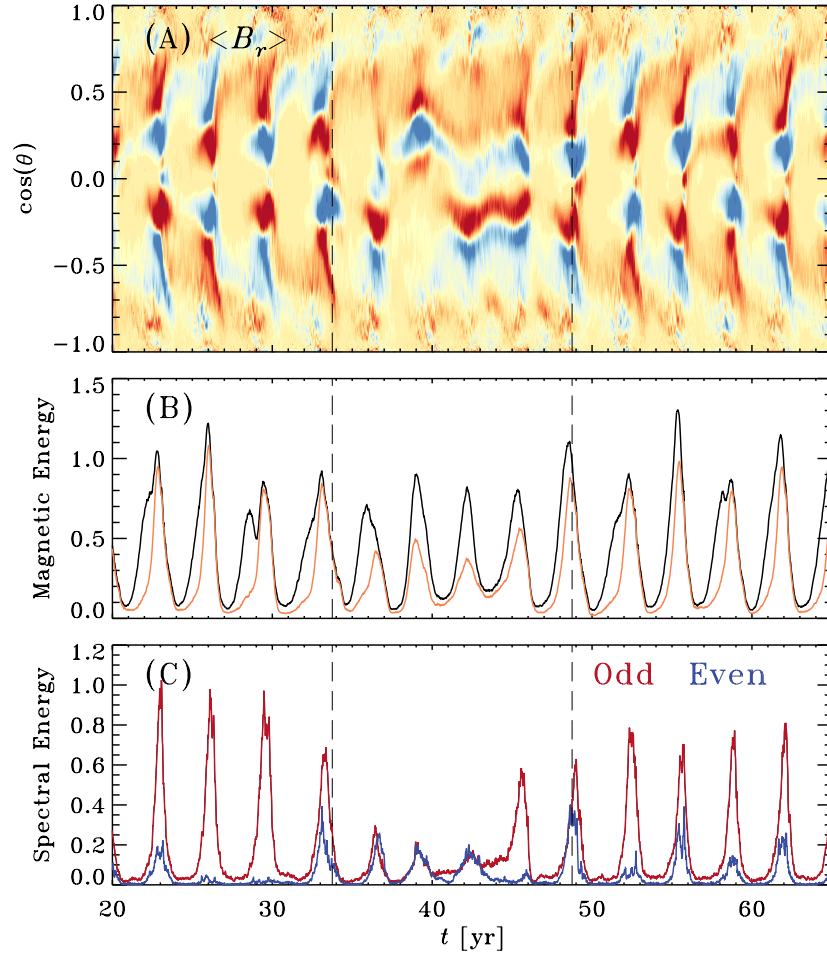


Figure 3.15 A Grand Minimum in the ASH K3S global MHD simulation of Augustson et al. (2015). The top panel is a time-latitude diagram of the zonally-averaged radial magnetic component at  $r/R = 0.75$ , near the base of the simulation domain. The color scale covers the range  $\pm 1$  kG from red to deep blue. The middle panel shows a time series of magnetic energy integrated over the simulation domain, and the bottom panel shows the corresponding time series of power in odd (red) and even (green) axisymmetric ( $m = 0$ ) spherical harmonics modes of the radial field decomposition at  $r/R = 0.75$ . The bipolar structures at low latitudes reflect the presence of equipartition-strength toroidal magnetic “wreaths” (Augustson et al., 2015). The vertical dashed line indicates the entry and exit from the Grand Minimum. Figure generated from numerical data kindly provided by K. Augustson.

{fig:K3S}

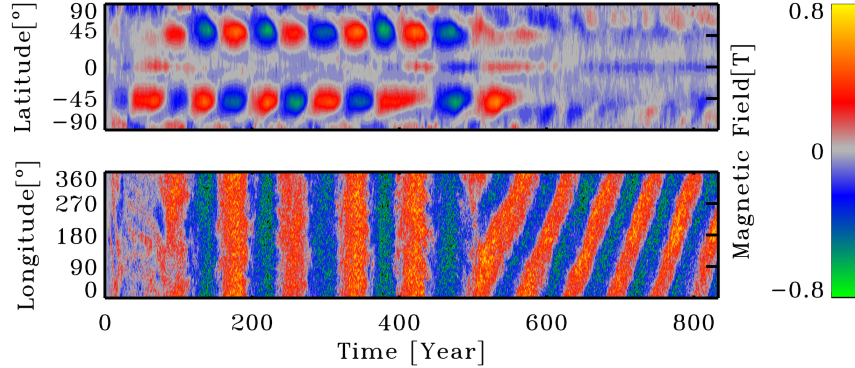


Figure 3.16 Dynamo mode transitions in a EULAG-MHD global simulation of convection and dynamo action, akin to the Passos and Charbonneau (2014) simulation discussed in §2.1. The top panel is a time-latitude diagram of the zonally averaged toroidal magnetic field at the base of the convecting layers ( $r/R = 0.71$ ), while the bottom panel displays a time-longitude diagram of the (unaveraged) toroidal magnetic component extracted at the same depth and latitude  $45^\circ$  North. The apparent disappearance of the large-scale magnetic cycle at  $t \simeq 500$  yr (top panel) is in fact due to the large-scale field transiting to a non-axisymmetric ( $m = 1$ ) “tilted dipole” configuration, still undergoing regular polarity reversals on a multi-decadal timescale (see text). Reproduced from Lawson et al. (2015) (Figure 14).

{fig:mhd70}

spatiotemporel evolution of the zonally-averaged toroidal magnetic component at the interface between the convectively unstable fluid and the underlying stably stratified fluid layer present in this simulation. A regular cycle showing good hemispheric synchrony and antisymmetric parity develops after about 100 yr of simulate time, and perdures for another 250 yr until the Southern hemisphere fails to reverse its polarity. The subsequent two (half-)cycles are then parity symmetric, but at  $t \simeq 500$  yr the Northern hemisphere shuts off, followed half a cycle later by the Southern hemisphere.

In fact, as shown on the bottom panel of Fig. 3.16, the large-scale magnetic cycle perdures through the end of this simulation, with roughly the same peak magnetic field strength and slightly reduced cycle period. What is plotted here is now a time-*longitude* diagram extracted at the same depth as the top panel and latitude  $45^\circ$  in the Northern hemisphere. It reveals that at  $t \simeq 500$  yr, what was up to then a cycling axisymmetric large-scale magnetic

field (no variation with longitude on global scales) transits abruptly to a non-axisymmetric configuration, which turns out to be well approximated by a dipole strongly tilted with respect to the rotation (symmetry) axis. This tilted dipole mode still undergoes regular polarity reversals, with a period only slightly shorter than its axisymmetric predecessor. The analysis of Lawson et al. (2015) suggests that this transition may be triggered by the development of a magnetoshear instability in the upper reaches of the stable fluid layer (on this see also Miesch, 2007; Gilman et al., 2007; Guerrero et al., 2016, and references therein).

The set of spherical wedge MHD simulations presented and analyzed in Viviani et al. (2018) also exhibits transition to non-axisymmetric, and further indicate that these become dominant at high rotation rates. Earlier similar simulations by Käpylä et al. (2016) illustrates yet another potentially relevant mechanism, namely the “destructive interference” between no less than three spatially segregated dynamo modes developing in their simulation (on co-existing dynamo modes in global MHD simulations see also Beaudoin et al., 2016).

{ssec:sumupcases}

### ***3.3.6 All together now***

Even the small set of case studies discussed in this section reveal an abundance of riches with regards to the means of generating Maunder Minimum-like epochs of strongly suppressed magnetic activity in extant dynamo models of the solar cycle. In what follows an attempt is made to identify some robust trends that persist across models.

In view of the strongly turbulent state of the solar convection zone, stochastic fluctuations in dynamo source terms appear inevitable, and these offer a simple means of generating long timescale fluctuations and Grand Minima/Maxima, in particular if the dynamo operates close to criticality; however, it is not at all obvious a priori whether or not the sun operates in this mildly supercritical regime. Convection itself is presumably strongly supercritical, but this does not imply that the dynamo process also is. One can find some observational support in the fact that the solar luminosity (and thus convective enthalpy flux) and differential rotation show very little variation in the course of the magnetic cycle, suggesting in turn that a weak backreaction on inductive flows. This is what one would (somewhat naively) expect from a mildly supercritical dynamo, unless amplitude saturation is entirely dominated by the constraint of magnetic helicity conservation.

Turning to strongly supercritical dynamos, deterministic nonlinear modulation of large-scale flows and interference between distinct dynamo

modes also emerges as a viable mechanism for long term modulation. The term “distinct” is to be understood as encompassing global modes differing and in equatorial and/or stapatially segragated local modes. Supercriticality is typically needed to avoid periodic or quasi-periodic modulation. An important caveat here relates to the fairly simplistic manner in which magnetic backreaction on large-scale flows is typically implemented in otherwise kinematic axisymmetric mean-field dynamo models. This failing remains particularly acute for flux transport dynamos.

At this writing, solar-like Grand Minima/Maxima have been and remain hard to produce in global MHD simulations of convection and dynamo action. The need to carry out temporally-extended simulation runs poses a obvious practical difficulty, but one can legitimately wonder whether there is more to it than that. Observationally, dipole reversal by the poleward transport of active region decay product appears to be an important component of the dynamo loop, yet there are no “active regions” in global simulations. Many such simulations also simulate only the convection zone, which de facto eliminates some potentially important inductive mechanism and dynamical effects.

The question can be turned around: can at least some long timescale variability scenarios be eliminated on the basis of extant data ? Here discriminant may be found in the manner different solar cycle models enter and exit Grand Minima. In most scenarios discussed in this section, recovery from a Grand Minimum is gradual, the return to “normal” cycle amplitudes taking place over a few magnetic cycles; this is not always the case (cf., e.g., Ossendrijver, 2000a, and Charbonneau et al. 2004). In some scenarios entry into Grand Minima takes place through a large excursion in cycle amplitude, while in other scenarios entry is as gradual as recovery (compare, e.g., Figs. 3.4 and 3.8 herein). Historical sunspot and auroral data (as well as yearly  $^{10}\text{Be}$  data) across the 1645–1715 Maunder Minimum could be crucial in this respect.

### 3.4 Can long-term variability be predicted ?

{sec:GMpredict}

As discussed in the next chapter, the prediction of solar Grand Minima and Maxima, and more generally of long timescale variability in overall activity levels, is becoming an important aspect of space climate modelling, and even of Earth’s climate modelling (Gray et al., 2010; Matthes et al., 2017). In light of the model results just discussed, this may appears hopeless task: not only do we not know which physical mechanism(s) drive long timescale variability, we do not even have a concensus model for the “basic” solar

magnetic cycle. Yet, the same model results indicates that prediction at some level may be possible.

Recent observational and modelling work indicates that the stochasticity of active region emergence poses strong limits to prediction, with a predictability window likely not exceeding a single (half)-cycle (Hathaway and Upton, 2016; Nagy et al., 2017; Labonville et al., 2019; Petrovay, 2020). Likewise, stochastically-driven intermittency (e.g., Figs. 3.3 and 3.7) is unpredictable, although short-term precursors may exist (more on this shortly). This, however, does not preclude prediction on long timescale, especially if long timescale variability is driven by deterministic nonlinear amplitude modulation. Looking for example at Figs. 3.12 and 3.13, there is clearly long-term “memory” in the amplitude modulation, with an associated predictability window largely exceeding the period of the primary cycle.

With regards to the prediction for the onset of Grand Minima, one precursor pattern emerges in a variety of models that rely on distinct basic dynamos and fluctuation mechanism: strong hemispheric asymmetry prior to onset (see Figs. 3.7, 3.9 and 3.15 herein). This can result from deterministic parity modulation, as well as from stochastic excitation of higher order dynamo modes.

chiefly: large hemispheric asymmetry in cycle preceding onset (point to Figs) reflecting parity modulation, or more generally, interaction of modes with distinct symmetries

GO effect

Kristof’s ARDoR

### 3.5 Summary

- There exist a wide variety of possible scenarios to push a solar/stellar dynamo in and out of quiescent epoch of strongly reduced or interrupted cyclic activity;
- purely deterministic nonlinear modulation tends to generate periodically or quasi-periodically recurring Grand Minima, often of similar duration;
- scenarios including stochastic mechanisms tend to produce aperiodically recurring Grand Minima with a wide distribution of durations;
- dynamo model subject to a lower operating threshold on field strength need a secondary dynamo to restart and exit from Grand Minima;
- some scenarios exhibit a precursor signal to the onset of grand minima (high cycle amplitude, pronounced GO signal, strong hemispheric asymmetry).
- ARDoR

## References

- Augustson, K., Brun, A. S., Miesch, M., and Toomre, J. 2015. Grand Minima and Equatorward Propagation in a Cycling Stellar Convective Dynamo. *Astrophys. J.*, **809**(Aug.), 149.
- Babcock, H.W. 1961. The Topology of the Sun's Magnetic Field and the 22-Year Cycle. *Astrophys. J.*, **133**, 572–589.
- Basu, Sarbani. 2016. Global seismology of the Sun. *Living Reviews in Solar Physics*, **13**(1), 2.
- Baumann, I., Schmitt, D., Schüssler, M., and Solanki, S. 2004. Evolution of the large-scale magnetic field on the solar surface: a parameter study. *Astron. Astrophys.*, **426**, 1075–1091.
- Beaudoin, P., Charbonneau, P., Racine, E., and Smolarkiewicz, P. K. 2013. Torsional Oscillations in a Global Solar Dynamo. *Solar Phys.*, **282**(Feb.), 335–360.
- Beaudoin, P., Simard, C., Cossette, J.-F., and Charbonneau, P. 2016. Double Dynamo Signatures in a Global MHD Simulation and Mean-field Dynamos. *Astrophys. J.*, **826**(Aug.), 138.
- Beer, J., Tobias, S., and Weiss, N. 1998. An Active Sun Throughout the Maunder Minimum. *Solar Phys.*, **181**(July), 237–249.
- Berger, Mitchell A. 1999. Introduction to magnetic helicity. *Plasma Physics and Controlled Fusion*, **41**(12B), B167–B175.
- Brandenburg, A. 2005. The Case for a Distributed Solar Dynamo Shaped by Near-Surface Shear. *Astrophys. J.*, **625**, 539–547.
- Brandenburg, A., and Subramanian, K. 2005. Astrophysical magnetic fields and nonlinear dynamo theory. *Phys. Rep.*, **417**, 1–209.
- Brandenburg, A., Rädler, K.-H., Rheinhardt, M., and Subramanian, K. 2008. Magnetic Quenching of  $\alpha$  and Diffusivity Tensors in Helical Turbulence. *Astrophys. J. Lett.*, **687**, L49–L52.
- Brandenburg, A., Candelaresi, S., and Chatterjee, P. 2009. Small-scale magnetic helicity losses from a mean-field dynamo. *Mon. Not. R. Astron. Soc.*, **398**(Sept.), 1414–1422.
- Brandenburg, Axel, and Sokoloff, Dmitry. 2002. Local and Nonlocal Magnetic Diffusion and Alpha-Effect Tensors in Shear Flow Turbulence. *Geophysical and Astrophysical Fluid Dynamics*, **96**(4), 319–344.
- Brooke, J., Moss, D., and Phillips, A. 2002. Deep minima in stellar dynamos. *Astronom. Astrophys.*, **395**(Dec.), 1013–1022.

- Brooke, J. M., Pelt, J., Tavakol, R., and Tworkowski, A. 1998. Grand minima and equatorial symmetry breaking in axisymmetric dynamo models. *Astronom. Astrophys.*, **332**(Apr.), 339–352.
- Brown, B. P., Miesch, M. S., Browning, M. K., Brun, A. S., and Toomre, J. 2011. Magnetic Cycles in a Convective Dynamo Simulation of a Young Solar-type Star. *Astrophys. J.*, **731**(Apr.), 69.
- Brown, B.P., Browning, M.K., Brun, A.S., Miesch, M.S., and Toomre, J. 2010. Persistent Magnetic Wreaths in a Rapidly Rotating Sun. *Astrophys. J.*, **711**, 424–438.
- Brown, T. M., Christensen-Dalsgaard, J., Dziembowski, W. A., Goode, P., Gough, D. O., and Morrow, C. A. 1989. Inferring the sun’s internal angular velocity from observed p-mode frequency splittings. *Astrophys. J.*, **343**(Aug.), 526–546.
- Browning, M.K., Miesch, M.S., Brun, A.S., and Toomre, J. 2006. Dynamo Action in the Solar Convection Zone and Tachocline: Pumping and Organization of Toroidal Fields. *Astrophys. J. Lett.*, **648**, L157–L160.
- Brun, A. S., Miesch, M. S., and Toomre, J. 2004. Global-Scale Turbulent Convection and Magnetic Dynamo Action in the Solar Envelope. *Astrophys. J.*, **614**(Oct.), 1073–1098.
- Bushby, P.J. 2006. Zonal flows and grand minima in a solar dynamo model. *Mon. Not. R. Astron. Soc.*, **371**, 772–780.
- Caligari, P., Moreno-Insertis, F., and Schüssler, M. 1995. Emerging flux tubes in the solar convection zone. I. Asymmetry, tilt, and emergence latitudes. *Astrophys. J.*, **441**, 886–902.
- Cameron, R., and Schüssler, M. 2007. Solar Cycle Prediction Using Precursors and Flux Transport Models. *Astrophys. J.*, **659**, 801–811.
- Cameron, R., and Schüssler, M. 2015. The crucial role of surface magnetic fields for the solar dynamo. *Science*, **347**(Mar.), 1333–1335.
- Cameron, R. H., and Schüssler, M. 2010. Changes of the Solar Meridional Velocity Profile During Cycle 23 Explained by Flows Toward the Activity Belts. *Astrophys. J.*, **720**(Sept.), 1030–1032.
- Cameron, R. H., and Schüssler, M. 2017a. An update of Leighton’s solar dynamo model. *Astronom. Astrophys.*, **599**(Mar.), A52.
- Cameron, R. H., and Schüssler, M. 2017b. Understanding Solar Cycle Variability. *Astrophys. J.*, **843**(July), 111.
- Cameron, R. H., Dasi-Espuig, M., Jiang, J., Işık, E., Schmitt, D., and Schüssler, M. 2013. Limits to solar cycle predictability: Cross-equatorial flux plumes. *Astron. Astrophys.*, **557**(Sep), A141.
- Cameron, R. H., Jiang, J., Schüssler, M., and Gizon, L. 2014. Physical causes of solar cycle amplitude variability. *Journal of Geophysical Research (Space Physics)*, **119**(Feb.), 680–688.
- Cattaneo, F., and Hughes, D. W. 1996. Nonlinear saturation of the turbulent  $\alpha$  effect. *Phys. Rev. Lett.*, **54**(Nov.), R4532–R4535.
- Cattaneo, Fausto. 1999. On the Origin of Magnetic Fields in the Quiet Photosphere. *Astrophys. J. Lett.*, **515**(1), L39–L42.
- Charbonneau, P. 2001. Multiperiodicity, Chaos, and Intermittency in a Reduced Model of the Solar Cycle. *Solar Phys.*, **199**(Apr.), 385–404.
- Charbonneau, P. 2005. A Maunder Minimum Scenario Based on Cross-Hemispheric Coupling and Intermittency. *Solar Phys.*, **229**, 345–358.
- Charbonneau, P. 2014. Solar Dynamo Theory. *Ann. Rev. Astron. Astrophys.*, **52**(Aug.), 251–290.

- Charbonneau, P., and Barlet, G. 2011. The dynamo basis of solar cycle precursor schemes. *Journal of Atmospheric and Solar-Terrestrial Physics*, **73**(Feb.), 198–206.
- Charbonneau, P., and Dikpati, M. 2000. Stochastic Fluctuations in a Babcock-Leighton Model of the Solar Cycle. *Astrophys. J.*, **543**(Nov.), 1027–1043.
- Charbonneau, P., and MacGregor, K. B. 1996. On the Generation of Equipartition-Strength Magnetic Fields by Turbulent Hydromagnetic Dynamos. *Astrophys. J. Lett.*, **473**(Dec.), L59.
- Charbonneau, P., Blais-Laurier, G., and St-Jean, C. 2004. Intermittency and Phase Persistence in a Babcock-Leighton Model of the Solar Cycle. *Astrophys. J. Lett.*, **616**(Dec.), L183–L186.
- Charbonneau, P., St-Jean, C., and Zacharias, P. 2005. Fluctuations in Babcock-Leighton Dynamos. I. Period Doubling and Transition to Chaos. *Astrophys. J.*, **619**(Jan.), 613–622.
- Charbonneau, P., Beaubien, G., and St-Jean, C. 2007. Fluctuations in Babcock-Leighton Dynamos. II. Revisiting the Gnevyshev-Ohl Rule. *Astrophys. J.*, **658**, 657–662.
- Charbonneau, Paul. 2013 (Jan). *Solar and Stellar Dynamos*. Saas-Fee Advanced Course.
- Chatterjee, P., Nandy, D., and Choudhuri, A. R. 2004. Full-sphere simulations of a circulation-dominated solar dynamo: Exploring the parity issue. *Astronom. Astrophys.*, **427**(Dec.), 1019–1030.
- Chatterjee, P., Mitra, D., Rheinhardt, M., and Brandenburg, A. 2011. Alpha effect due to buoyancy instability of a magnetic layer. *Astronom. Astrophys.*, **534**(Oct.), A46.
- Cheung, M. C. M., Rempel, M., Title, A. M., and Schüssler, M. 2010. Simulation of the Formation of a Solar Active Region. *Astrophys. J.*, **720**(1), 233–244.
- Cheung, Mark C. M., and Isobe, Hiroaki. 2014. Flux Emergence (Theory). *Living Reviews in Solar Physics*, **11**(1), 3.
- Childress, Stephen, and Gilbert, Andrew D. 1995. *Stretch, Twist, Fold*.
- Choudhuri, A. R. 1992. Stochastic fluctuations of the solar dynamo. *Astronom. Astrophys.*, **253**(Jan.), 277–285.
- Choudhuri, A. R., and Gilman, P. A. 1987. The influence of the Coriolis force on flux tubes rising through the solar convection zone. *Astrophys. J.*, **316**(May), 788–800.
- Choudhuri, A. R., and Karak, B. B. 2012. Origin of Grand Minima in Sunspot Cycles. *Physical Review Letters*, **109**(17), 171103.
- Choudhuri, A. R., Schüssler, M., and Dikpati, M. 1995. The solar dynamo with meridional circulation. *Astronom. Astrophys.*, **303**(Nov.), L29.
- Cole, L. C., and Bushby, P. J. 2014. Modulated cycles in an illustrative solar dynamo model with competing  $\alpha$ -effects. *Astronom. Astrophys.*, **563**(Mar.), A116.
- Cossette, J.-F., Charbonneau, P., and Smolarkiewicz, P. K. 2013. Cyclic Thermal Signature in a Global MHD Simulation of Solar Convection. *Astrophys. J. Lett.*, **777**(Nov.), L29.
- Covas, E., Tavakol, R., and Moss, D. 2001. Dynamical variations of the differential rotation in the solar convection zone. *Astronom. Astrophys.*, **371**(May), 718–730.

- Dasi-Espuig, M., Solanki, S. K., Krivova, N. A., Cameron, R., and Peñuela, T. 2010. Sunspot group tilt angles and the strength of the solar cycle. *Astronom. Astrophys.*, **518**(July), A7.
- Davidson, P.A. 2001. *An Introduction to Magnetohydrodynamics*. Cambridge Texts in Applied Mathematics. Cambridge; New York: Cambridge University Press.
- DeVore, C. R., Boris, J. P., and Sheeley, N. R., Jr. 1984. The concentration of the large-scale solar magnetic field by a meridional surface flow. *Solar Phys.*, **92**(1-2), 1–14.
- Dikpati, M., and Charbonneau, P. 1999. A Babcock-Leighton Flux Transport Dynamo with Solar-like Differential Rotation. *Astrophys. J.*, **518**(June), 508–520.
- Dikpati, M., and Gilman, P.A. 2001. Flux-Transport Dynamos with  $\alpha$ -Effect from Global Instability of Tachocline Differential Rotation: A Solution for Magnetic Parity Selection in the Sun. *Astrophys. J.*, **559**, 428–442.
- Dikpati, M., de Toma, G., Gilman, P. A., Arge, C. N., and White, O. R. 2004. Diagnostics of Polar Field Reversal in Solar Cycle 23 Using a Flux Transport Dynamo Model. *Astrophys. J.*, **601**(Feb.), 1136–1151.
- D’Silva, S., and Choudhuri, A.R. 1993. A theoretical model for tilts of bipolar magnetic regions. *Astron. Astrophys.*, **272**, 621–633.
- Duarte, L. D. V., Wicht, J., Browning, M. K., and Gastine, T. 2016. Helicity inversion in spherical convection as a means for equatorward dynamo wave propagation. *Mon. Not. R. Astron. Soc.*, **456**(Feb.), 1708–1722.
- Dubé, Caroline, and Charbonneau, Paul. 2013. Stellar Dynamos and Cycles from Numerical Simulations of Convection. *Astrophys. J.*, **775**(1), 69.
- Durney, B. R. 1995. On a Babcock-Leighton dynamo model with a deep-seated generating layer for the toroidal magnetic field. *Solar Phys.*, **160**(Sept.), 213–235.
- Durney, B. R. 1997. On a Babcock-Leighton Solar Dynamo Model with a Deep-seated Generating Layer for the Toroidal Magnetic Field. IV. *Astrophys. J.*, **486**(Sept.), 1065–1077.
- Durney, B. R. 2000. On the Differences Between Odd and Even Solar Cycles. *Solar Phys.*, **196**(Oct.), 421–426.
- Fan, Y. 2009. Magnetic Fields in the Solar Convection Zone. *Living Rev. Solar Phys.*, **6**.
- Fan, Y., and Fang, F. 2014. A Simulation of Convective Dynamo in the Solar Convective Envelope: Maintenance of the Solar-like Differential Rotation and Emerging Flux. *Astrophys. J.*, **789**(July), 35.
- Fan, Y., Fisher, G.H., and Deluca, E.E. 1993. The origin of morphological asymmetries in bipolar active regions. *Astrophys. J.*, **405**, 390–401.
- Fan, Y., Fisher, G. H., and McClymont, A. N. 1994. Dynamics of emerging active region flux loops. *Astrophys. J.*, **436**(Dec.), 907–928.
- Featherstone, N. A., and Miesch, M. S. 2015. Meridional Circulation in Solar and Stellar Convection Zones. *Astrophys. J.*, **804**(May), 67.
- Ferriz-Mas, A., Schmitt, D., and Schüssler, M. 1994. A dynamo effect due to instability of magnetic flux tubes. *Astron. Astrophys.*, **289**, 949–956.
- Gastine, T., Yadav, R. K., Morin, J., Reiners, A., and Wicht, J. 2014. From solar-like to antisolar differential rotation in cool stars. *Mon. Not. R. Astron. Soc.*, **438**(Feb.), L76–L80.
- Ghizaru, M., Charbonneau, P., and Smolarkiewicz, P.K. 2010. Magnetic cycles in global large eddy simulations of solar convection. *Astrophys. J. Lett.*, in press.

- Gilman, P. A. 1983. Dynamically consistent nonlinear dynamos driven by convection in a rotating spherical shell. II - Dynamos with cycles and strong feedbacks. *Astrophys. J. Suppl.*, **53**(Oct.), 243–268.
- Gilman, P. A., and Rempel, M. 2005. Concentration of Toroidal Magnetic Field in the Solar Tachocline by  $\eta$ -Quenching. *Astrophys. J.*, **630**(Sept.), 615–622.
- Gilman, P. A., Dikpati, M., and Miesch, M. S. 2007. Global MHD Instabilities in a Three-dimensional Thin-Shell Model of Solar Tachocline. *Astrophys. J. Suppl.*, **170**(May), 203–227.
- Glatzmaier, G. A. 1984. Numerical simulations of stellar convective dynamos. I - The model and method. *Journal of Computational Physics*, **55**(Sept.), 461–484.
- Glatzmaier, G.A. 1985. Numerical simulations of stellar convective dynamos. II. Field propagation in the convection zone. *Astrophys. J.*, **291**, 300–307.
- Gray, L. J., Beer, J., Geller, M., Haigh, J. D., Lockwood, M., Matthes, K., Cubasch, U., Fleitmann, D., Harrison, G., Hood, L., Luterbacher, J., Meehl, G. A., Shindell, D., van Geel, B., and White, W. 2010. Solar Influences on Climate. *Reviews of Geophysics*, **48**(4), RG4001.
- Guerrero, G., and de Gouveia Dal Pino, E.M. 2008. Turbulent magnetic pumping in a Babcock-Leighton solar dynamo model. *Astron. Astrophys.*, **485**, 267–273.
- Guerrero, G., Dikpati, M., and de Gouveia Dal Pino, E. M. 2009. The Role of Diffusivity Quenching in Flux-transport Dynamo Models. *Astrophys. J.*, **701**(Aug.), 725–736.
- Guerrero, G., Smolarkiewicz, P. K., Kosovichev, A. G., and Mansour, N. N. 2013. Differential Rotation in Solar-like Stars from Global Simulations. *Astrophys. J.*, **779**(Dec.), 176.
- Guerrero, G., Smolarkiewicz, P. K., de Gouveia Dal Pino, E. M., Kosovichev, A. G., and Mansour, N. N. 2016. On the Role of Tachoclines in Solar and Stellar Dynamos. *Astrophys. J.*, **819**(Mar.), 104.
- Guerrero, G., Zaire, B., Smolarkiewicz, P. K., de Gouveia Dal Pino, E. M., Kosovichev, A. G., and Mansour, N. N. 2019. What Sets the Magnetic Field Strength and Cycle Period in Solar-type Stars? *Astrophys. J.*, **880**(1), 6.
- Hale, G. E., Ellerman, F., Nicholson, S. B., and Joy, A. H. 1919. The Magnetic Polarity of Sun-Spots. *Astrophys. J.*, **49**(Apr.), 153.
- Hathaway, D. H. 2012. Supergranules as Probes of the Sun’s Meridional Circulation. *Astrophys. J.*, **760**(Nov.), 84.
- Hathaway, D. H., and Upton, L. A. 2016. Predicting the amplitude and hemispheric asymmetry of solar cycle 25 with surface flux transport. *Journal of Geophysical Research (Space Physics)*, **121**(10), 10.
- Hazra, G., Karak, B. B., and Choudhuri, A. R. 2014a. Is a Deep One-cell Meridional Circulation Essential for the Flux Transport Solar Dynamo? *Astrophys. J.*, **782**(Feb.), 93.
- Hazra, G., Karak, B. B., Banerjee, D., and Choudhuri, A. R. 2015. Correlation Between Decay Rate and Amplitude of Solar Cycles as Revealed from Observations and Dynamo Theory. *Solar Phys.*, **290**(June), 1851–1870.
- Hazra, G., Choudhuri, A. R., and Miesch, M. S. 2017. A Theoretical Study of the Build-up of the Sun’s Polar Magnetic Field by using a 3D Kinematic Dynamo Model. *Astrophys. J.*, **835**(Jan.), 39.
- Hazra, S., Passos, D., and Nandy, D. 2014b. A Stochastically Forced Time Delay Solar Dynamo Model: Self-consistent Recovery from a Maunder-like Grand

- Minimum Necessitates a Mean-field Alpha Effect. *Astrophys. J.*, **789**(July), 5.
- Hazra, Soumitra, and Nandy, Dibyendu. 2019. The origin of parity changes in the solar cycle. *Mon. Not. R. Astron. Soc.*, **489**(3), 4329–4337.
- Hotta, H., and Yokoyama, T. 2010a. Importance of Surface Turbulent Diffusivity in the Solar Flux-Transport Dynamo. *Astrophys. J.*, **709**(Feb.), 1009–1017.
- Hotta, H., and Yokoyama, T. 2010b. Solar Parity Issue with Flux-transport Dynamo. *Astrophys. J. Lett.*, **714**(May), L308–L312.
- Hotta, H., Rempel, M., and Yokoyama, T. 2015. Efficient Small-scale Dynamo in the Solar Convection Zone. *Astrophys. J.*, **803**(1), 42.
- Hotta, H., Rempel, M., and Yokoyama, T. 2016. Large-scale magnetic fields at high Reynolds numbers in magnetohydrodynamic simulations. *Science*, **351**(Mar.), 1427–1430.
- Howe, R. 2009. Solar Interior Rotation and its Variation. *Living Rev. Solar Phys.*, **6**.
- Hoyng, P. 1988. Turbulent transport of magnetic fields. III. Stochastic excitation of global magnetic modes. *Astrophys. J.*, **332**, 857–871.
- Hoyng, P. 1993. Helicity fluctuations in mean field theory: an explanation for the variability of the solar cycle? *Astron. Astrophys.*, **272**, 321–339.
- Hoyng, P., Schmitt, D., and Teuben, L. J. W. 1994. The effect of random alpha-fluctuations and the global properties of the solar magnetic field. *Astronom. Astrophys.*, **289**(Sept.), 265–278.
- Jackiewicz, J., Serebryanskiy, A., and Kholikov, S. 2015. Meridional Flow in the Solar Convection Zone. II. Helioseismic Inversions of GONG Data. *Astrophys. J.*, **805**(June), 133.
- Jennings, R.L., and Weiss, N.O. 1991. Symmetry breaking in stellar dynamos. *Mon. Not. R. Astron. Soc.*, **252**, 249–260.
- Jha, Bibhuti Kumar, Karak, Bidya Binay, Mandal, Sudip, and Banerjee, Dipankar. 2020. Magnetic Field Dependence of Bipolar Magnetic Region Tilts on the Sun: Indication of Tilt Quenching. *Astrophys. J. Lett.*, **889**(1), L19.
- Jiang, J., Chatterjee, P., and Choudhuri, A.R. 2007. Solar activity forecast with a dynamo model. *Mon. Not. R. Astron. Soc.*, **381**, 1527–1542.
- Jiang, J., Cameron, R. H., Schmitt, D., and Schüssler, M. 2011. The solar magnetic field since 1700. I. Characteristics of sunspot group emergence and reconstruction of the butterfly diagram. *Astronom. Astrophys.*, **528**(Apr.), A82.
- Jiang, J., Cameron, R. H., Schmitt, D., and İşik, E. 2013. Modeling solar cycles 15 to 21 using a flux transport dynamo. *Astronom. Astrophys.*, **553**(May), A128.
- Jiang, J., Hathaway, D. H., Cameron, R. H., Solanki, S. K., Gizon, L., and Upton, L. 2014. Magnetic Flux Transport at the Solar Surface. *Space Sci. Rev.*, **186**(Dec.), 491–523.
- Jouve, L., and Brun, A.S. 2007. On the role of meridional flows in flux transport dynamo models. *Astron. Astrophys.*, **474**, 239–250.
- Jouve, L., Brown, B.P., and Brun, A.S. 2010. Exploring the  $P_{cyc}$  vs.  $P_{rot}$  relation with flux transport dynamo models of solar-like stars. *Astron. Astrophys.*, **509**, A32.
- Käpylä, M. J., Käpylä, P. J., Olsper, N., Brandenburg, A., Warnecke, J., Karak, B. B., and Pelt, J. 2016. Multiple dynamo modes as a mechanism for long-term solar activity variations. *Astronom. Astrophys.*, **589**(May), A56.

- Käpylä, P. J., Mantere, M. J., and Brandenburg, A. 2012. Cyclic Magnetic Activity due to Turbulent Convection in Spherical Wedge Geometry. *Astrophys. J. Lett.*, **755**(Aug.), L22.
- Käpylä, P. J., Mantere, M. J., Cole, E., Warnecke, J., and Brandenburg, A. 2013. Effects of Enhanced Stratification on Equatorward Dynamo Wave Propagation. *Astrophys. J.*, **778**(Nov.), 41.
- Käpylä, P. J., Viviani, M., Käpylä, M. J., Brandenburg, A., and Spada, F. 2019. Effects of a subadiabatic layer on convection and dynamos in spherical wedge simulations. *Geophysical and Astrophysical Fluid Dynamics*, **113**(1-2), 149–183.
- Käpylä, P.J., Korpi, M.J., Brandenburg, A., Mitra, D., and Tavakol, R. 2010. Convective dynamos in spherical wedge geometry. *Astron. Nachr.*, **331**, 73.
- Karak, B. B. 2010. Importance of Meridional Circulation in Flux Transport Dynamo: The Possibility of a Maunder-like Grand Minimum. *Astrophys. J.*, **724**(Dec.), 1021–1029.
- Karak, B. B., and Choudhuri, A. R. 2011. The Waldmeier effect and the flux transport solar dynamo. *Mon. Not. R. Astron. Soc.*, **410**(Jan.), 1503–1512.
- Karak, B. B., and Choudhuri, A. R. 2012. Quenching of Meridional Circulation in Flux Transport Dynamo Models. *Solar Phys.*, **278**(May), 137–148.
- Karak, B. B., and Choudhuri, A. R. 2013. Studies of grand minima in sunspot cycles by using a flux transport solar dynamo model. *Research in Astronomy and Astrophysics*, **13**(Nov.), 1339–1357.
- Karak, B. B., and Nandy, D. 2012. Turbulent Pumping of Magnetic Flux Reduces Solar Cycle Memory and thus Impacts Predictability of the Sun’s Activity. *Astrophys. J. Lett.*, **761**(Dec.), L13.
- Karak, B. B., Rheinhardt, M., Brandenburg, A., Käpylä, P. J., and Käpylä, M. J. 2014. Quenching and Anisotropy of Hydromagnetic Turbulent Transport. *Astrophys. J.*, **795**(Nov.), 16.
- Karak, Bidya Binay, and Miesch, Mark. 2017. Solar Cycle Variability Induced by Tilt Angle Scatter in a Babcock-Leighton Solar Dynamo Model. *Astrophys. J.*, **847**(1), 69.
- Kitchatinov, L. L., and Olemskoy, S. V. 2012. Solar Dynamo Model with Diamagnetic Pumping and Nonlocal  $\alpha$ -Effect. *Solar Phys.*, **276**(Feb.), 3–17.
- Kitchatinov, L. L., Pipin, V. V., Makarov, V. I., and Tlatov, A. G. 1999. Solar torsional oscillations and the grand activity cycle. *Solar Phys.*, **189**(Nov.), 227–239.
- Kitchatinov, L. L., Mordvinov, A. V., and Nepomnyashchikh, A. A. 2018. Modelling variability of solar activity cycles. *Astronom. Astrophys.*, **615**(July), A38.
- Kitchatinov, L.L., and Rüdiger, G. 1993.  $\Lambda$ -effect and differential rotation in stellar convection zones. *Astron. Astrophys.*, **276**, 96–102.
- Kitchatinov, L.L., Rüdiger, G., and Küker, M. 1994.  $\Lambda$ -quenching as the nonlinearity in stellar-turbulence dynamos. *Astron. Astrophys.*, **292**, 125–132.
- Kitchatinov, L.L., Mazur, M.V., and Jardine, M. 2000. Magnetic field escape from a stellar convection zone and the dynamo-cycle period. *Astron. Astrophys.*, **359**, 531–538.
- Knobloch, E., and Landsberg, A. S. 1996. A new model of the solar cycle. *Mon. Not. R. Astron. Soc.*, **278**(1), 294–302.
- Knobloch, E., Tobias, S.M., and Weiss, N.O. 1998. Modulation and symmetry changes in stellar dynamos. *Mon. Not. R. Astron. Soc.*, **297**, 1123–1138.

- Krause, F., and Rädler, K.-H. 1980. *Mean-Field Magnetohydrodynamics and Dynamo Theory*. Oxford; New York: Pergamon Press.
- Kueker, M., Ruediger, G., and Pipin, V. V. 1996. Solar torsional oscillations due to the magnetic quenching of the Reynolds stress. *Astronom. Astrophys.*, **312**(Aug.), 615–623.
- Küker, M., Arlt, R., and Rüdiger, R. 1999. The Maunder minimum as due to magnetic  $\Lambda$ -quenching. *Astron. Astrophys.*, **343**, 977–982.
- Küker, M., Rüdiger, G., and Schulz, M. 2001. Circulation-dominated solar shell dynamo models with positive alpha effect. *Astron. Astrophys.*, **374**, 301–308.
- Labonville, Francois, Charbonneau, Paul, and Lemerle, Alexandre. 2019. A Dynamo-based Forecast of Solar Cycle 25. *Solar Phys.*, **294**(6), 82.
- Lawson, N., Strugarek, A., and Charbonneau, P. 2015. Evidence of Active MHD Instability in EULAG-MHD Simulations of Solar Convection. *Astrophys. J.*, **813**(Nov.), 95.
- Leighton, R.B. 1964. Transport of magnetic fields on the sun. *Astrophys. J.*, **140**, 1547–1562.
- Leighton, R.B. 1969. A magneto-kinematic model of the solar cycle. *Astrophys. J.*, **156**, 1–26.
- Lemerle, A., and Charbonneau, P. 2017. A Coupled 2×2D Babcock-Leighton Solar Dynamo Model. II. Reference Dynamo Solutions. *Astrophys. J.*, **834**(Jan.), 133.
- Lemerle, A., Charbonneau, P., and Carignan-Dugas, A. 2015. A Coupled 2×2D Babcock-Leighton Solar Dynamo Model. I. Surface Magnetic Flux Evolution. *Astrophys. J.*, **810**(Sept.), 78.
- Longcope, D. W., and Fisher, G. H. 1996. The Effects of Convection Zone Turbulence on the Tilt Angles of Magnetic Bipoles. *Astrophys. J.*, **458**(Feb.), 380.
- Lopes, I., and Passos, D. 2009. Solar Variability Induced in a Dynamo Code by Realistic Meridional Circulation Variations. *Solar Phys.*, **257**, 1–12.
- Lopes, I., Passos, D., Nagy, M., and Petrovay, K. 2014. Oscillator Models of the Solar Cycle. Towards the Development of Inversion Methods. *Space Sci. Rev.*, **186**(Dec.), 535–559.
- Mabuchi, J., Masada, Y., and Kageyama, A. 2015. Differential Rotation in Magnetized and Non-magnetized Stars. *Astrophys. J.*, **806**(June), 10.
- MacGregor, K.B., and Charbonneau, P. 1997. Solar interface dynamos. I. Linear, kinematic models in cartesian geometry. *Astrophys. J.*, **486**, 484–501.
- Mandal, K., Hanasoge, S. M., Rajaguru, S. P., and Antia, H. M. 2018. Helioseismic Inversion to Infer the Depth Profile of Solar Meridional Flow Using Spherical Born Kernels. *Astrophys. J.*, **863**(1), 39.
- Markiel, J.A., and Thomas, J.H. 1999. Solar interface dynamo models with a realistic rotation profile. *Astrophys. J.*, **523**, 827–837.
- Masada, Y., Yamada, K., and Kageyama, A. 2013. Effects of Penetrative Convection on Solar Dynamo. *Astrophys. J.*, **778**(Nov.), 11.
- Mason, J., Hughes, D.W., and Tobias, S.M. 2002. The competition in the solar dynamo between surface and deep-seated  $\alpha$ -effect. *Astrophys. J. Lett.*, **580**, L89–L92.
- Matthes, Katja, Funke, Bernd, Andersson, Monika E., Barnard, Luke, Beer, Jürg, Charbonneau, Paul, Clilverd, Mark A., Dudok de Wit, Thierry, Haberleiter, Margit, Hendry, Aaron, Jackman, Charles H., Kretzschmar, Matthieu, Kruschke, Tim, Kunze, Markus, Langematz, Ulrike, Marsh, Daniel R., Maycock,

- Amanda C., Misios, Stergios, Rodger, Craig J., Scaife, Adam A., Seppälä, Annika, Shangguan, Ming, Sinnhuber, Miriam, Tourpali, Kleareti, Usoskin, Ilya, van de Kamp, Max, Verronen, Pekka T., and Versick, Stefan. 2017. Solar forcing for CMIP6 (v3.2). *Geoscientific Model Development*, **10**(6), 2247–2302.
- McClintock, B. H., and Norton, A. A. 2013. Recovering Joy’s Law as a Function of Solar Cycle, Hemisphere, and Longitude. *Solar Phys.*, **287**(Oct.), 215–227.
- Miesch, M. S. 2007. Sustained Magnetoshear Instabilities in the Solar Tachocline. *Astrophys. J. Lett.*, **658**(Apr.), L131–L134.
- Miesch, M. S., and Dikpati, M. 2014. A Three-dimensional Babcock-Leighton Solar Dynamo Model. *Astrophys. J. Lett.*, **785**(Apr.), L8.
- Miesch, M. S., and Teweldebirhan, K. 2016. A three-dimensional Babcock-Leighton solar dynamo model: Initial results with axisymmetric flows. *Advances in Space Research*, **58**(Oct.), 1571–1588.
- Miesch, M. S., Brun, A. S., and Toomre, J. 2006. Solar Differential Rotation Influenced by Latitudinal Entropy Variations in the Tachocline. *Astrophys. J.*, **641**(Apr.), 618–625.
- Miesch, M.S. 2005. Large-Scale Dynamics of the Convection Zone and Tachocline. *Living Rev. Solar Phys.*, **2**.
- Miesch, M.S., and Toomre, J. 2009. Turbulence, Magnetism, and Shear in Stellar Interiors. *Annual Review of Fluid Mechanics*, **41**, 317–345.
- Mininni, P.D., and Gómez, D.O. 2002. Study of Stochastic Fluctuations in a Shell Dynamo. *Astrophys. J.*, **573**, 454–463.
- Mininni, P.D., and Gómez, D.O. 2004. A new technique for comparing solar dynamo models and observations. *Astron. Astrophys.*, **426**, 1065–1073.
- Moffatt, H.K. 1978. *Magnetic Field Generation in Electrically Conducting Fluids*. Cambridge Monographs on Mechanics and Applied Mathematics. Cambridge; New York: Cambridge University Press.
- Moffatt, Keith, and Dormy, Emmanuel. 2019. *Self-Excited Fluid Dynamos*. Cambridge; New York: Cambridge University Press.
- Moreno-Insertis, F. 1986. Nonlinear time-evolution of kink-unstable magnetic flux tubes in the convective zone of the sun. *Astrophys. J.*, **166**, 291–305.
- Moss, D., and Brooke, J.M. 2000. Towards a model of the solar dynamo. *Mon. Not. R. Astron. Soc.*, **315**, 521–533.
- Moss, D., Tuominen, I., and Brandenburg, A. 1990. Buoyancy-limited thin-shell dynamos. *Astron. Astrophys.*, **240**, 142–149.
- Moss, D., Brandenburg, A., Tavakol, R., and Tuominen, I. 1992. Stochastic effects in mean-field dynamos. *Astronom. Astrophys.*, **265**(Nov.), 843–849.
- Moss, D., Sokoloff, D., Usoskin, I., and Tutubalin, V. 2008. Solar Grand Minima and Random Fluctuations in Dynamo Parameters. *Solar Phys.*, **250**, 221–234.
- Muñoz-Jaramillo, A., Nandy, D., Martens, P. C. H., and Yeates, A. R. 2010. A Double-ring Algorithm for Modeling Solar Active Regions: Unifying Kinematic Dynamo Models and Surface Flux-transport Simulations. *Astrophys. J. Lett.*, **720**(Sept.), L20–L25.
- Muñoz-Jaramillo, A., Nandy, D., and Martens, P.C.H. 2009. Helioseismic Data Inclusion in Solar Dynamo Models. *Astrophys. J.*, **698**, 461–478.
- Nagy, M., Lemerle, A., Labonville, F., Petrovay, K., and Charbonneau, P. 2017. The Effect of “Rogue” Active Regions on the Solar Cycle. *Solar Phys.*, **292**(Nov.), 167.

- Nandy, D., and Choudhuri, A.R. 2001. Toward a mean-field formulation of the Babcock–Leighton type solar dynamo. I.  $\alpha$ -coefficient versus Durney’s doubling approach. *Astrophys. J.*, **551**, 576–585.
- Nelson, N. J., Brown, B. P., Brun, A. S., Miesch, M. S., and Toomre, J. 2013. Magnetic Wreaths and Cycles in Convective Dynamos. *Astrophys. J.*, **762**(Jan.), 73.
- Nelson, N. J., Brown, B. P., Sacha Brun, A., Miesch, M. S., and Toomre, J. 2014. Buoyant Magnetic Loops Generated by Global Convective Dynamo Action. *Solar Phys.*, **289**(Feb.), 441–458.
- Ölçek, Deniz, Charbonneau, Paul, Lemerle, Alexand re, Longpré, Gabriel, and Boileau, Florence. 2019. Grand Activity Minima and Maxima via Dual Dynamos. *Solar Phys.*, **294**(7), 99.
- Olemskoy, S. V., and Kitchatinov, L. L. 2013. Grand Minima and North-South Asymmetry of Solar Activity. *Astrophys. J.*, **777**(Nov.), 71.
- Ossendrijver, A.J.H., Hoyng, P., and Schmitt, D. 1996. Stochastic excitation and memory of the solar dynamo. *Astron. Astrophys.*, **313**, 938–948.
- Ossendrijver, M. 2003. The solar dynamo. *Astron. Astrophys. Rev.*, **11**, 287–367.
- Ossendrijver, M.A.J.H. 2000a. The dynamo effect of magnetic flux tubes. *Astron. Astrophys.*, **359**, 1205–1210.
- Ossendrijver, M.A.J.H. 2000b. Grand minima in a buoyancy-driven solar dynamo. *Astron. Astrophys.*, **359**, 364–372.
- Ossendrijver, M.A.J.H., and Hoyng, P. 1996. Stochastic and nonlinear fluctuations in a mean field dynamo. *Astron. Astrophys.*, **313**, 959–970.
- Ossendrijver, M.A.J.H., Stix, M., and Brandenburg, A. 2001. Magnetoconvection and dynamo coefficients: dependence of the  $\alpha$ -effect on rotation and magnetic fields. *Astron. Astrophys.*, **376**, 713–726.
- Otmianowska-Mazur, K., Rüdiger, G., Elstner, D., and Arlt, R. 1997. The turbulent EMF as a time series and the ‘quality’ of dynamo cycles. *Geophys. Astrophys. Fluid Dyn.*, **86**, 229–247.
- Parker, E. N. 1979. *Cosmical magnetic fields: Their origin and their activity.*
- Parker, E.N. 1955. Hydromagnetic Dynamo Models. *Astrophys. J.*, **122**, 293–314.
- Parker, E.N. 1975. The Generation of Magnetic Fields in Astrophysical Bodies. X. Magnetic Buoyancy and the Solar Dynamo. *Astrophys. J.*, **198**, 205–209.
- Parker, E.N. 1993. A solar dynamo surface wave at the interface between convection and nonuniform rotation. *Astrophys. J.*, **408**, 707–719.
- Passos, D., and Charbonneau, P. 2014. Characteristics of magnetic solar-like cycles in a 3D MHD simulation of solar convection. *Astronom. Astrophys.*, **568**(Aug.), A113.
- Passos, D., and Lopes, I. 2011. Grand minima under the light of a low order dynamo model. *Journal of Atmospheric and Solar-Terrestrial Physics*, **73**(Feb.), 191–197.
- Passos, D., Charbonneau, P., and Beaudoin, P. 2012. An Exploration of Non-kinematic Effects in Flux Transport Dynamos. *Solar Phys.*, **279**(July), 1–22.
- Passos, D., Nandy, D., Hazra, S., and Lopes, I. 2014. A solar dynamo model driven by mean-field alpha and Babcock-Leighton sources: fluctuations, grand-minima-maxima, and hemispheric asymmetry in sunspot cycles. *Astronom. Astrophys.*, **563**(Mar.), A18.
- Passos, D., Charbonneau, P., and Miesch, M. 2015. Meridional Circulation Dynamics from 3D Magnetohydrodynamic Global Simulations of Solar Convection. *Astrophys. J. Lett.*, **800**(Feb.), L18.

- Passos, D., Miesch, M., Guerrero, G., and Charbonneau, P. 2017. Meridional circulation dynamics in a cyclic convective dynamo. *Astronom. Astrophys.*, **607**(Nov.), A120.
- Petrovay, K. 2010. Solar Cycle Prediction. *Living Reviews in Solar Physics*, **7**(Dec.), 6.
- Petrovay, Kristóf. 2020. Solar cycle prediction. *Living Reviews in Solar Physics*, **17**(1), 2.
- Pevtsov, A. A., Berger, M. A., Nindos, A., Norton, A. A., and van Driel-Gesztelyi, L. 2014. Magnetic Helicity, Tilt, and Twist. *Space Sci. Rev.*, **186**(Dec.), 285–324.
- Phillips, J.A., Brooke, J.M., and Moss, D. 2002. The importance of physical structure in solar dynamo models. *Astron. Astrophys.*, **392**, 713–727.
- Pipin, V. V., and Kosovichev, A. G. 2011a. Mean-field Solar Dynamo Models with a Strong Meridional Flow at the Bottom of the Convection Zone. *Astrophys. J.*, **738**(Sept.), 104.
- Pipin, V. V., and Kosovichev, A. G. 2011b. The Asymmetry of Sunspot Cycles and Waldmeier Relations as a Result of Nonlinear Surface-shear Shaped Dynamo. *Astrophys. J.*, **741**(Nov.), 1.
- Pipin, V. V., Sokoloff, D. D., and Usoskin, I. G. 2012. Variations of the solar cycle profile in a solar dynamo with fluctuating dynamo governing parameters. *Astronom. Astrophys.*, **542**(June), A26.
- Pipin, V.V. 1999. The Gleissberg cycle by a nonlinear  $\alpha\Lambda$  dynamo. *Astron. Astrophys.*, **346**, 295–302.
- Platt, N., Spiegel, E.A., and Tresser, C. 1993. On-off intermittency: A mechanism for bursting. *Phys. Rev. Lett.*, **70**, 279–282.
- Pouquet, A., Frish, U., and Leorat, J. 1976. Strong MHD helical turbulence and the nonlinear dynamo effect. *J. Fluid Mech.*, **77**, 321–354.
- Racine, É., Charbonneau, P., Ghizaru, M., Bouchat, A., and Smolarkiewicz, P. K. 2011. On the Mode of Dynamo Action in a Global Large-eddy Simulation of Solar Convection. *Astrophys. J.*, **735**(July), 46.
- Rajaguru, S. P., and Antia, H. M. 2015. Meridional Circulation in the Solar Convection Zone: Time-Distance Helioseismic Inferences from Four Years of HMI/SDO Observations. *Astrophys. J.*, **813**(Nov.), 114.
- Rempel, M. 2005a. Influence of Random Fluctuations in the  $\Lambda$ -Effect on Meridional Flow and Differential Rotation. *Astrophys. J.*, **631**(Oct.), 1286–1292.
- Rempel, M. 2005b. Solar Differential Rotation and Meridional Flow: The Role of a Subadiabatic Tachocline for the Taylor-Proudman Balance. *Astrophys. J.*, **622**(Apr.), 1320–1332.
- Rempel, M. 2006. Flux-Transport Dynamos with Lorentz Force Feedback on Differential Rotation and Meridional Flow: Saturation Mechanism and Torsional Oscillations. *Astrophys. J.*, **647**, 662–675.
- Rempel, M. 2014. Numerical Simulations of Quiet Sun Magnetism: On the Contribution from a Small-scale Dynamo. *Astrophys. J.*, **789**(2), 132.
- Rempel, M. 2018. Small-scale Dynamo Simulations: Magnetic Field Amplification in Exploding Granules and the Role of Deep and Shallow Recirculation. *Astrophys. J.*, **859**(2), 161.
- Rempel, M., and Cheung, M. C. M. 2014. Numerical Simulations of Active Region Scale Flux Emergence: From Spot Formation to Decay. *Astrophys. J.*, **785**(2), 90.

- Rempel, M., and Schüssler, M. 2001. Intensification of magnetic fields by conversion of potential energy. *Astrophys. J. Lett.*, **552**, L171–L174.
- Roald, C. B. 1998. A two-layer alpha-omega-dynamo model with dynamic feedback on the omega-effect. *Mon. Not. R. Astron. Soc.*, **300**(Oct.), 397–410.
- Roald, C.B., and Thomas, J.H. 1997. Simple solar dynamo models with variable  $\alpha$  and  $\omega$  effects. *Mon. Not. R. Astron. Soc.*, **288**, 551–564.
- Rüdiger, G., and Hollerbach, R. 2004. *The magnetic universe : geophysical and astrophysical dynamo theory*.
- Ruediger, G., and Arlt, R. 1996. Cycle times and magnetic amplitudes in nonlinear 1D  $\alpha^2\Omega$ -dynamoes. *Astronom. Astrophys.*, **316**(Dec.), L17–L20.
- Schad, A., Timmer, J., and Roth, M. 2013. Global Helioseismic Evidence for a Deeply Penetrating Solar Meridional Flow Consisting of Multiple Flow Cells. *Astrophys. J. Lett.*, **778**(Dec.), L38.
- Schatten, K.H., Scherrer, P.H., Svalgaard, L., and Wilcox, J.M. 1978. Using dynamo theory to predict the sunspot number during solar cycle 21. *Geophys. Res. Lett.*, **5**, 411–414.
- Schmalz, S., and Stix, M. 1991. An  $\alpha\Omega$  dynamo with order and chaos. *Astron. Astrophys.*, **245**, 654–661.
- Schmitt, D., and Schüssler, M. 1989. Non-linear dynamo I. One-dimensional model of a thin layer dynamo. *Astron. Astrophys.*, **223**, 343–351.
- Schmitt, D., Schüssler, M., and Ferriz-Mas, A. 1996. Intermittent solar activity by an on-off dynamo. *Astron. Astrophys.*, **311**, L1–L4.
- Schrijver, C.J., DeRosa, M.L., and Title, A.M. 2002. What Is Missing from Our Understanding of Long-Term Solar and Heliospheric Activity? *Astrophys. J.*, **577**, 1006–1012.
- Schrinner, M., Rädler, K.-H., Schmitt, D., Rheinhardt, M., and Christensen, U. R. 2007. Mean-field concept and direct numerical simulations of rotating magnetoconvection and the geodynamo. *Geophysical and Astrophysical Fluid Dynamics*, **101**(Apr.), 81–116.
- Simard, C., Charbonneau, P., and Dubé, C. 2016. Characterisation of the turbulent electromotive force and its magnetically-mediated quenching in a global EULAG-MHD simulation of solar convection. *Advances in Space Research*, **58**(Oct.), 1522–1537.
- Simard, Corinne, and Charbonneau, Paul. 2020. Grand Minima in a spherical non-kinematic  $\alpha^2\Omega$  mean-field dynamo model. *Journal of Space Weather and Space Climate*, **10**(Jan.), 9.
- Simitev, R. D., Kosovichev, A. G., and Busse, F. H. 2015. Dynamo Effects Near the Transition from Solar to Anti-Solar Differential Rotation. *Astrophys. J.*, **810**(Sept.), 80.
- Sokoloff, D., and Nesme-Ribes, E. 1994. The Maunder minimum: A mixed-parity dynamo mode? *Astron. Astrophys.*, **288**, 293–298.
- Spiegel, E.A., and Zahn, J.-P. 1992. The solar tachocline. *Astron. Astrophys.*, **265**, 106–114.
- Stein, R. F., and Nordlund, Å. 2006. Solar Small-Scale Magnetoconvection. *Astrophys. J.*, **642**(2), 1246–1255.
- Stein, Robert F. 2012. Solar Surface Magneto-Convection. *Living Reviews in Solar Physics*, **9**(1), 4.
- Stein, Robert F., and Nordlund, Åke. 2012. On the Formation of Active Regions. *Astrophys. J. Lett.*, **753**(1), L13.

- Stejko, Andrey M., Guerrero, Gustavo, Kosovichev, Alexander G., and Smolarkiewicz, Piotr K. 2020. 3D MHD Modeling of the Impact of Subsurface Stratification on the Solar Dynamo. *Astrophys. J.*, **888**(1), 16.
- Stenflo, J. O., and Kosovichev, A. G. 2012. Bipolar Magnetic Regions on the Sun: Global Analysis of the SOHO/MDI Data Set. *Astrophys. J.*, **745**(Feb.), 129.
- Stix, M. 1976. Differential Rotation and the Solar Dynamo. *Astron. Astrophys.*, **47**, 243–254.
- Strugarek, A., Beaudoin, P., Charbonneau, P., Brun, A. S., and do Nascimento, J.-D. 2017. Reconciling solar and stellar magnetic cycles with nonlinear dynamo simulations. *Science*, **357**(July), 185–187.
- Strugarek, A., Beaudoin, P., Charbonneau, P., and Brun, A. S. 2018. On the Sensitivity of Magnetic Cycles in Global Simulations of Solar-like Stars. *Astrophys. J.*, **863**(1), 35.
- Svalgaard, L., Cliver, E. W., and Kamide, Y. 2005. Sunspot cycle 24: Smallest cycle in 100 years? *Geophys. Res. Lett.*, **32**(Jan.), L01104.
- Thelen, J.-C. 2000. A mean electromotive force induced by magnetic buoyancy instabilities. *Mon. Not. R. Astron. Soc.*, **315**, 155–164.
- Tlatova, Ksenia, Tlatov, Andrey, Pevtsov, Alexei, Mursula, Kalevi, Vasil’eva, Valeria, Heikkinen, Elina, Bertello, Luca, Pevtsov, Alexander, Virtanen, Ilpo, and Karachik, Nina. 2018. Tilt of Sunspot Bipoles in Solar Cycles 15 to 24. *Solar Phys.*, **293**(8), 118.
- Tobias, S. M., Weiss, N. O., and Kirk, V. 1995. Chaotically modulated stellar dynamos. *Mon. Not. R. Astron. Soc.*, **273**(Apr.), 1150–1166.
- Tobias, S. M., Cattaneo, F., and Brummell, N. H. 2011. On the Generation of Organized Magnetic Fields. *Astrophys. J.*, **728**(2), 153.
- Tobias, S.M. 1996. Diffusivity quenching as a mechanism for Parker’s surface dynamo. *Astrophys. J.*, **467**, 870–880.
- Tobias, S.M. 1997. The solar cycle: parity interactions and amplitude modulation. *Astron. Astrophys.*, **322**, 1007–1017.
- Workowski, A., Tavakol, R., Brandenburg, A., Brooke, J.M., Moss, D., and Tuominen, I. 1998. Intermittent behaviour in axisymmetric mean-field dynamo models in spherical shells. *Mon. Not. R. Astron. Soc.*, **296**, 287–295.
- Upton, L., and Hathaway, D. H. 2014. Predicting the Sun’s Polar Magnetic Fields with a Surface Flux Transport Model. *Astrophys. J.*, **780**(Jan.), 5.
- Usoskin, I.G., Sokoloff, D., and Moss, D. 2009. Grand Minima of Solar Activity and the Mean-Field Dynamo. *Solar Phys.*, **254**, 345–355.
- Viviani, M., Warnecke, J., Käpylä, M. J., Käpylä, P. J., Olsper, N., Cole-Kodikara, E. M., Lehtinen, J. J., and Brandenburg, A. 2018. Transition from axisymmetric to nonaxisymmetric dynamo modes in spherical convection models of solar-like stars. *Astronom. Astrophys.*, **616**(Aug.), A160.
- Viviani, M., Käpylä, M. J., Warnecke, J., Käpylä, P. J., and Rheinhardt, M. 2019. Stellar Dynamos in the Transition Regime: Multiple Dynamo Modes and Antisolar Differential Rotation. *Astrophys. J.*, **886**(1), 21.
- Vögler, A., and Schüssler, M. 2007. A solar surface dynamo. *Astronom. Astrophys.*, **465**(3), L43–L46.
- Wang, Y. M., and Sheeley, N. R., Jr. 1989. Average Properties of Bipolar Magnetic Regions during Sunspot CYCLE-21. *Solar Phys.*, **124**(1), 81–100.
- Wang, Y.-M., and Sheeley Jr, N.R. 1991. Magnetic flux transport and the sun’s dipole moment - New twists to the Babcock-Leighton model. *Astrophys. J.*, **375**, 761–770.

- Wang, Y.-M., Nash, A.G., and Sheeley Jr, N.R. 1989. Magnetic flux transport on the sun. *Science*, **245**, 712–718.
- Wang, Y.-M., Sheeley Jr, N.R., and Nash, A.G. 1991. A new cycle model including meridional circulation. *Astrophys. J.*, **383**, 431–442.
- Warnecke, J. 2018. Dynamo cycles in global convection simulations of solar-like stars. *Astronom. Astrophys.*, **616**(Aug.), A72.
- Warnecke, J., Käpylä, P. J., Käpylä, M. J., and Brandenburg, A. 2014. On The Cause of Solar-like Equatorward Migration in Global Convective Dynamo Simulations. *Astrophys. J. Lett.*, **796**(Nov.), L12.
- Warnecke, J., Rheinhardt, M., Tuomisto, S., Käpylä, P. J., Käpylä, M. J., and Brandenburg, A. 2016. Turbulent transport coefficients in spherical wedge dynamo simulations of solar-like stars. *ArXiv e-prints*, Jan.
- Warnecke, J., Rheinhardt, M., Tuomisto, S., Käpylä, P. J., Käpylä, M. J., and Brandenburg, A. 2018. Turbulent transport coefficients in spherical wedge dynamo simulations of solar-like stars. *Astron. Astrophys.*, **609**(Jan), A51.
- Weber, M. A., Fan, Y., and Miesch, M. S. 2013. Comparing Simulations of Rising Flux Tubes Through the Solar Convection Zone with Observations of Solar Active Regions: Constraining the Dynamo Field Strength. *Solar Phys.*, **287**(Oct.), 239–263.
- Weiss, N. O., and Tobias, S. M. 2016. Supermodulation of the Sun’s magnetic activity: the effects of symmetry changes. *Mon. Not. R. Astron. Soc.*, **456**(Mar.), 2654–2661.
- Wilmot-Smith, A.L., Nandy, D., Hornig, G., and Martens, P.C.H. 2006. A Time Delay Model for Solar and Stellar Dynamos. *Astrophys. J.*, **652**, 696–708.
- Yadav, R. K., Gastine, T., Christensen, U. R., and Duarte, L. D. V. 2013. Consistent Scaling Laws in Anelastic Spherical Shell Dynamos. *Astrophys. J.*, **774**(Sept.), 6.
- Yeates, A. R., and Muñoz-Jaramillo, A. 2013. Kinematic active region formation in a three-dimensional solar dynamo model. *Mon. Not. R. Astron. Soc.*, **436**(Dec.), 3366–3379.
- Yeates, A.R., Nandy, D., and Mackay, D.H. 2008. Exploring the Physical Basis of Solar Cycle Predictions: Flux Transport Dynamics and Persistence of Memory in Advection- versus Diffusion-dominated Solar Convection Zones. *Astrophys. J.*, **673**, 544–556.
- Yoshimura, H. 1975. Solar-cycle dynamo wave propagation. *Astrophys. J.*, **201**, 740–748.
- Yoshimura, H. 1978. Nonlinear astrophysical dynamos: Multiple-period dynamo wave oscillations and long-term modulations of the 22 year solar cycle. *Astrophys. J.*, **226**, 706–719.
- Yoshimura, H. 1981. Solar cycle Lorentz force waves and the torsional oscillations of the sun. *Astrophys. J.*, **247**(Aug.), 1102–1112.
- Zhao, J., Bogart, R. S., Kosovichev, A. G., Duvall, Jr., T. L., and Hartlep, T. 2013. Detection of Equatorward Meridional Flow and Evidence of Double-cell Meridional Circulation inside the Sun. *Astrophys. J. Lett.*, **774**(Sept.), L29.